Remote sensing of two exceptional winter aerosol pollution events and representativeness of ground-based measurements

Alexandre Baron, Patrick Chazette, Julien Totems

Laboratoire des Sciences du Climat et de l'Environnement, LSCE-IPSL, CEA-CNRS-UVSQ, UMR 8212, Gif-sur-Yvette, France

Correspondence to: Alexandre Baron (alexandre.baron@lsce.ipsl.fr)

Abstract. Two intense winter aerosol pollution events, which took place in winter 2016-2017 in Paris, were monitored using a ground-based N_2-Raman lidar, in the framework of WASLIP (Winter Aerosol Survey by Lidar In Paris), a dedicated field campaign that was carried out in this area from 1 November 2016 to 31 January 2017. The data analysis uses the synergy between ground-based and spaceborne lidar observations, and data from the air quality monitoring network Airparif. The first severe aerosol pollution event began on 30 November 2016 and ended on 2 December, concerning a circular area of ~250 km in diameter around Paris. The maximum PM_{10} was $121\pm63\mu g$ m^{-3} (regional spatial average $\pm$ standard deviation) for the Airparif ground-based PM monitoring stations and the aerosol extinction coefficient (AEC) ranged from 0.2 to 1 km^{-1}. The second event took place from 20 to 23 January which covered all of the North-western Europe, with maxima of PM_{10} around 156 ± 33 μg m^{-3} and AEC between 0.6 and 1 km^{-1}, within the winter atmospheric boundary layer. Although these two major aerosol pollution events did not occur under identical anticyclonic weather conditions, they share very low planetary boundary layer (PBL) heights, down to 300 m above ground level. However, they. Moreover, they are associated with significantly different aerosol lidar ratios: 72 ± 15 sr and 56 ± 15 sr, respectively in December and January. Such results are consistent with available spaceborne lidar data, 70 ± 25 sr from CALIOP (Cloud Aerosol Lidar and Infrared Pathfinder Satellite Observations), and values found in the literature. During these two events, the continuous temporal evolution of the aerosol extinction coefficient allows us to investigate the representativeness of optical parameters found in the planetary boundary layer to assess surface aerosol concentration. No one-to-one relationship between the aerosol optical thickness (AOT) and $PM_{2.5}$ values stands out within our study. In contrast, the maximum aerosol extinction coefficient found within the planetary boundary layer correlates well with $PM_{2.5}$ at ground ($R^2\sim0.75$, specific extinction cross-section of 9.4 m^2 g^{-1}) for these polluted events. Thus this lidar-derived aerosol extinction coefficient is identified as a consistent variable to monitor the pollution during winter events.

Keywords: lidar, aerosols, spaceborne, AOT, $PM_{2.5}$, winter, urban, pollution.

1 Introduction

According to the report of the Organization for Economic Co-operation and Development (OECD), particulate matter (PM) is one of the main anthropogenic factors affecting human health and agriculture (OECD, 2016). Indirectly, this pollution induces substantial economic tolls: the same report claims that global healthcare costs related to air pollution rose to USD 21 billion in 2015 and projections reach up to USD 176 billion by 2060. Furthermore, aerosols are responsible for a significant decrease in life expectancy in large urban and industrial areas (IIASA, 2000). Whereas they represent a small portion of the cumulative exposure of an urban dweller, severe aerosol pollution events are known for their important short-term impact on human health and especially excess mortality in at-risk populations (Hogg and Van Eeden, 2009). Once advected in the atmosphere, their effects on health and climate (IPCC, 2013) extend from regional to global scale.

Places where inhabitants are the most concerned and vulnerable to particulate pollution are megacities (Molina and Molina, 2004). Thus, several studies were performed in such conurbations in order to investigate the aerosol impacts on air quality and climate, such as in Mexico in 2016 with the Megacity Initiative: Local and Global Research Observations (MILAGRO, Molina et al., 2010) or in California during California Nexus (CalNex, e.g. Hersey et al., 2013). International field experiments were also carried out in Europe as well as in the United Kingdom, with the M25 (ring-road around London) experiment (McMeeking et al., 2012), or in southern France with the Expérience sur Site pour Contraindre les Modèles de Pollution atmosphérique et de Transport d'Emissions (ESCOMPTE, Cros et al., 2004). Nevertheless, air quality remains a great challenge to resolve in the future as the European Commission estimates that 90% of EU citizens are regularly exposed to air pollutant levels above the World Health Organization (WHO) guidelines (European Commission, 2015).

Being one of the densest urban areas in Europe, with more than 18% of the French population concentrated in 2.2% of its metropolitan territory (Pereira et al., 2013; Ile de France Prefecture, 2017), the Paris megacity (Paris city limits extended to all its suburbs in the Ile-de-France region) is often concerned by air pollution issues. Several field campaigns have been conducted in the Paris area: the Etude et Simulation de la QUalité de l'air en Ile-de-France project (ESQUIF, Vautard et al., 2003; Chazette et al., 2005; Hodzic et al., 2006), LIdar pour la Surveillance de L'AIR (LISAIR, Raut and Chazette, 2007) and The Megacities: Emissions, urban, regional and Global Atmospheric POLlution and climate effects, and Integrated tools for assessment and mitigation project (MEGAPOLI, e.g. Von Der Weiden-Reinmüller et al., 2014; Freney et al., 2014). These campaigns allowed to assess the environmental impacts of the Paris megacity (Skyllakou et al., 2014) mainly during summer and improved the predictability (Beekmann, 2003; Tombette et al., 2009; Royer et al., 2011b) and the source apportionment of aerosol pollution events (Sciare et al., 2010; Crippa et al., 2013a; Bressi et al., 2013, 2014; Pikridas et al., 2015). So far, existing studies of winter aerosol pollution events (APEs) in Paris were mainly derived from modelling (Bessagnet et al., 2005; Crippa et al., 2013b; Beekmann et al., 2015). They demonstrate that in weather-blocking conditions and with a cold surface, the PBL height is low, and therefore the vertical dispersion of pollution is poor, resulting in forecast uncertainties (e.g. Steeneveld, 2011).

The use of *in situ* sounding or lidar remote sensing techniques which enable a high vertical resolution can provide valuable data to air pollution models. Establishing a relationship between particle concentration at ground level and optical observations

within the PBL may enhance the predictability of air pollution peaks and improve the assessment of air quality on a continental scale (Wang et al., 2013). Many authors seek to derive such a relationship between $PM_{2.5}$ and optical observations, mainly performed from satellites, as shown in the recent review study of Chu et al. (2016).

Hence, the main purpose of this paper is to describe the meteorological conditions that prevail during the two significant winter APEs, to characterize observed APEs using in situ and remote sensing data and finally to investigate the link between ground-based aerosol concentrations and optical properties of particles trapped within the winter PBL. This study is based on a specific field campaign performed during the most severe winter APEs that occurred in the Paris area since 2009. The need for such a study to enhance the accuracy of $PM_{2.5}$ assessment using surface aerosol extinction is clearly identified in the conclusion of Toth et al. (2014), opening the way for more accurate assessments of air quality on a global scale with the upcoming new generation of both ground-based (e.g. ref earlynet) and spaceborne lidar, such as those carried onboard ADM-Aeolus (Flamant et al., 2008) and further the European spaceborne mission EarthCARE (Illingworth et al., 2015).

To draw a relationship between surface concentration of aerosol and their optical properties within the PBL, the following approach is used in this paper: i) lidar measurements are inverted in order to retrieve aerosol optical properties, such as the lidar ratio (LR) and the aerosol extinction coefficient (AEC), ii) the linear particle depolarization ratio (LPDR) is then assessed and used along with the LR to identify the aerosol typing, iii) the meteorological situation is examined to identify the origin of pollution aerosol over the Paris area, iv) spaceborne observations are used when available to corroborate the meteorological analysis and give a regional view of pollution plume and, v) the link between the aerosol optical properties within the PBL and the ground-based particulate matter is studied.

Section 2 presents the instrumentation and datasets involved in the study. Passive and active remote sensing measurements are mainly used, completed by meteorological model outputs and the dataset of the Airparif air quality measuring network. We highlight the most polluted winter days of the past decade in Section 3 from archived ground-based PM_{10} measurements and analyse the associated weather situations. In Section 4 we analyse in depth the measurements performed during winter 2016/2017, which included those of a N_2-Raman ground-based lidar. This period was associated with two exceptional APEs whose characteristics are described in Section 5: we take advantage of the entire lidar dataset of these APEs. It covers a wide range of aerosol load, from pollution free days to severely polluted days. These data are analysed in terms of correlation between ground level and aerosol optical properties within the PBL using Airparif PM measurements and lidar vertical profiles, respectively. Finally, Section 6 concludes this paper by summarizing the main results.

2 Methodology and tools

This section presents the instruments and tools used during and following the field campaign held from November 2016 to the end of January 2017.

2.1 Ground-based lidar measurements and analysis

In the framework of the WASLIP campaign, the compact 355 nm Lidar for Automatic Atmospheric Surveys Using Raman Scattering (LAASURS) was deployed close to the centre of Paris at the QualAir station (http://qualair.aero.jussieu.fr/) located on the rooftop of the Paris Sorbonne University Jussieu Campus (48° 50′ 50″ N, 2° 21′ 20″ E), ~100 m above mean sea level (AMSL). This experimental site is part of the OSU EcceTerra (http://ecceterra.sorbonne-universite.fr/fr/index.html) and has been set-up by the Laboratoire d'Etudes du Rayonnement et de la Matière en Astrophysique et Atmosphères (LERMA) and Laboratoire ATmosphères, Milieux, Observations Spatiales (LATMOS) essentially for atmospheric studies. The LAASURS has been successfully involved in former field campaigns as in Chazette and Totems (2017), Dieudonné et al. (2015, 2017), and it is extensively described in Royer et al. (2011a).

2.1.1 Technical characteristics

The LAASURS has been developed at LSCE for ground-based or airborne aerosol remote sensing in the field. The reception is composed of three channels, two using elastic scattering filtered at 354.7±0.1 nm and separated into parallel and perpendicular polarizations of light with respect to the laser emission, as well as a third channel using the inelastic nitrogen vibrational Raman scattering induced by the laser and filtered at 387.6±0.1 nm (Chazette et al., 2016). The three channels provide measurements from their short overlap distance of ~150 m up to 20 km. The overlap factor is calculated during night time using a horizontal line of sigh as described in Chazette et al., (2007) assuming a homogeneous layer of aerosols from the emission to 1.5 km horizontal distance. In the lowermost 150 m, the uncertainties induced by the overlap factor do not permit to assess aerosol optical properties with a sufficient level of confidence. The emission is provided by an Ultra® Nd:YAG laser manufactured by Quantel delivering 6-7 ns pulses of 30 mJ at a 20 Hz frequency. The initial vertical and temporal resolutions of the lidar are respectively 0.75 m and 50 s (1000 laser shots averaged). More characteristics are given in Table 1 and the casing enclosing the lidar is presented in Figure 1.

2.1.2 Inversion of lidar profiles

To obtain a sufficient signal to noise ratio (SNR, SNR > 10 (Royer et al., 2011a)) from the N_2-Raman channel during daytime, the vertical resolution is set to 15 m and lidar profiles are averaged over 10 minutes. Two methods can be used to retrieve the aerosol optical parameters: i) A synergy between the elastic channels and a sun-photometer as in Chazette (2003), Pahlow et al.(2006), Raut and Chazette(2007) and Cuesta et al.(2008); or, ii) the use of a N_2-Raman channel as described in Russo et al. (2006), Ansmann et al. (2008) or Royer et al. (2011a). In this work, the presence of the N_2-Raman channel of the LAASURS makes it preferable to use the second approach detailed by Royer et al. (2011a) and Chazette et al. (2017). Readers can refer to these articles. During daytime, the lidar-derived AOT is checked against the one measured by the sun-photometer of the AERONET Paris site at concomitant times. The AOTs, combined with the elastic channel, lead to the retrieval of the aerosol extinction and backscatter coefficient profiles (AEC and ABC, respectively), and to their ratio, also called lidar ratio (LR). In

the inversion process, the extrapolation of AOT measurements from the N_2-Raman wavelength to the elastic wavelength assumes a constant Ångström exponent with height for the particles in the atmospheric column, furthermore a mean value of the Ångström exponent is taken for each APE. The Ångström exponent is derived from the AErosol RObotic NETwork database (AERONET, http://aeronet.gsfc.nasa.gov/) for the Paris site. The assumption of constant exponent in altitude is

5   consistent as all aerosols are concentrated in a well-mixed shallow PBL. In addition, AERONET data shows a temporal variability during each APE below ±0.5. The LR may vary as well in the atmospheric column since different types of aerosols can be present. However, in the particular case of this work, with most of the particles trapped close to ground level in a winter PBL, the assumption of an equivalent LR for the entire column is justified. When the aerosol load is sufficient (ABC 5% above the molecular backscatter coefficient), the linear particulate depolarization ratio (LPDR) is computed as in Chazette et al.

10   (2012).

2.1.3 Uncertainties

The different sources of uncertainties for our lidar system are discussed in Royer et al. (2011a) where the authors used a Monte Carlo method applied to the direct-inverse model of the lidar to obtain its error budget. These uncertainties are strongly dependent on the SNR. The SNR encountered in these measurements (signal originating from the lower troposphere: altitude

15   < 2-3 km AMSL) remains greater than 10. In these conditions, the relative uncertainty on the N_2-Raman-derived AOT is less than 2%. The relative uncertainties on the LR and AEC vary from 7% and 3%, respectively, for AOT greater than 0.5. They increase to 23% and 13%, respectively, for AOT ~ 0.1 (see Table 2 in Royer et al. (2011a)). We can consider a standard deviation of 10 sr on the LR for AOT ≳ 0.2. The constant Ångström exponent assumption with an input incertitude of ±0.5 will induce uncertainties of 4% on the LR and 1.5% on the AEC as calculated by Royer et al. (2011a). Relative uncertainties

20   on the LPDR retrieval are discussed in Dieudonné et al. (2015; 2017) and are of the same magnitude as those associated to the LR. For small LPDR values (< 5%), the absolute error is between 1 and 2 %.

Table 1: LAASURS characteristics

Emission wavelength	354,7 nm
Laser energy	30 mJ
Pulse duration	6-7 ns
Shooting frequency	20 Hz
Emission lens diameter	Ø 50 mm
Reception lens diameter	Ø 150 mm
Field of view	2 x 0,67 mrad
Complete overlap distance	150m to 200 m
Elastic channels wavelength	354.7±0.1 nm
Raman N_2 channel wavelength	387.6±0.1 nm
Detector	Photomultiplier
Acquisition mode	Analog and photon count
Acquisition frequency	200 MHz
Spatial resolution	0.75 m to 15 m

Figure 1: LAASURS system on the Paris Sorbonne University rooftop

2.2 Spaceborne instruments

2.2.1 MODIS

On-board both Terra and Aqua satellites, the Moderate Resolution Imaging Spectroradiometer (MODIS) (Salomonson et al., 1989; King et al., 1992; Remer et al., 2005) is composed of 36 spectral bands ranging from 400 nm to 1440 nm. Its swath is 110° (2330 km) and the resolution at ground level varies from 250 m to 1000 m, depending on the band used. Here we use the AOT at 550 nm included in the collection 6 (C6) deep blue aerosol products MOD04_L2 and MYD04_L2 (Levy et al., 2013). The predicted uncertainty over land on the AOT at 550 nm remains as in collection 5 (C5): ±0.05+0.15 AOT (Levy et al., 2010).

2.2.2 CALIOP

Launched in April 2006 to be part of the A-Train (Stephens et al., 2002), the Cloud Aerosol Lidar and Infrared Pathfinder Satellite Observations (CALIPSO) is a satellite carrying a backscatter lidar for atmospheric observations purposes. The spaceborne Cloud-Aerosol LIdar with Orthogonal Polarization (CALIOP) is composed of a diode-pumped Nd:YAG emitting 110 mJ linearly polarized pulses at a repetition rate of 20.25 Hz at both 1064 nm and 532 nm wavelengths (Winker et al., 2003). Horizontal and vertical resolutions are respectively 333 m and 30 to 60 m. Here we take advantage of its level 2 V4.20 operational products (Mamouri et al., 2009) when the CALIPSO track passes above the Paris area (within 200 km).

2.2.3 CATS

The spaceborne lidar Cloud-Aerosol Transport System (CATS, https://cats.gsfc.nasa.gov/) was operating on-board the International Space Station (ISS) from January 2015 to October 2017. CATS has been recently evaluated by ground-based lidar measurements from the EARLINET network (Proestakis et al., 2019). The data used in this work come from the mode

5   7.2 HSRL Demo of the CATS mission. Namely, this acquisition mode uses the backscattered light emitted at 532 and 1064 nm and the depolarization of the 1064 nm channel. In this study, we use the operational product of version L2O_V3-00 (NASA, 2017) with aerosol typing based on lidar ratio considerations. It comes as a complement to CALIOP data, strengthening the credibility of their concomitant results.

Note that CALIOP and CATS have a different typology for aerosol subtyping and associated lidar ratio. Readers can find in

10   (Kim et al., 2018) the selection algorithm used for CALIOP data version 4 and in (Yorks et al., 2015) the theoretical basis of CATS algorithm. For the *polluted continental/ smoke* aerosol subtype, CALIOP and CATS give a LR of 70±25 sr and 65 sr, respectively.

2.3 Ground-based networks and model outputs

2.3.1 AERONET

15   The AErosol RObotic NETwork (AERONET, https://aeronet.gsfc.nasa.gov/) is a global network of automatic sun-photometers (Holben et al., 1998). The sun- and sky-scanning provide long-term and continuous monitoring of aerosol optical, microphysical, and radiative properties. The current processing algorithms are in their third version and composed of three quality levels: 1.0 (unscreened), 1.5 (cloud-screened and quality controlled) and 2.0 (quality-assured). The uncertainty on AOT is 0.01 for wavelength $\lambda > 440$ nm (Holben et al., 1998) and up to 0.02 for other wavelengths (Dubovik et al., 2000), but

20   additional bias may appear in presence of thin unscreened cirrus (Chew et al., 2011). To prevent this, we use level 2.0 products and we highlight the presence of clouds in lidar vertical profiles.

2.3.2 Airparif

Airparif's mission is to monitor the air quality in the region of Paris, and to inform citizens and authorities if regulatory thresholds on several gaseous or PM pollution are exceeded. These thresholds are taken from two EU directives (n°

25   2008/50/CE and 2004/107/CE) transposed into French law. We consider the annual average limits for PM_{10} and $PM_{2.5}$, (40 µg m^{-3} and 25 µg m^{-3}, respectively) as well as the information and the alert thresholds for PM_{10} (50 µg m^{-3} and 80 µg m^{-3}, respectively).

The ground-based stations included in the Airparif network are divided into two main categories: the traffic and the background stations. Then, the background stations are split in three sub-types: urban, sub-urban and rural stations according to their

30   geographical location in the Paris region. Here, only these background stations are considered for the winter months of December, January and February. Fourteen stations measure PM_{10} whereas only nine measure $PM_{2.5}$ in 2017; these numbers

have varied over the past years and are taken into account when calculating uncertainties on the spatial average. Only dry PM are measured using a Tapered Element Oscillating Microbalance (TEOM), as the sampling is performed through a warmed inlet. On a daily average, the uncertainty associated with this measure is within 9% - 16% for $PM_{2.5}$ and 9% - 21.6% for PM_{10} over the studied period (http://www.airparif.asso.fr/telechargement/telechargement-statistique).

5   **2.3.3 ECMWF ERA5 reanalysis**

Used for a better understanding of the weather situation from a synoptic point of view, the meteorological data in this paper comes from the European Centre for Medium-Range Weather Forecasts (ECMWF) and more precisely their fifth generation of atmospheric reanalyses of the global climate: ERA5 (ECMWF, 2017). We use reanalyses with a spatial resolution of 0.25° latitude x 0.25° longitude on 37 pressure levels, which are produced every hour.

10   **3 Major winter pollution events of the past decade (2007-2017)**

3.1 Identification from ground-level in situ sampling

The time series of PM_{10} between December 2007 and February 2018 (www.airparif.asso.fr/en) over the Ile-de-France region are investigated. The identification of the main APEs is performed in three steps: i) as legal thresholds for population information and alert are based on daily mean PM values, a daily average is computed for each background station; ii) we

15   select the days during which at least one background station exceeds the PM_{10} information threshold of 50 µg m^{-3} or the alert threshold of 80 µg m^{-3}. iii) To single out the most polluted regional-scale events of the past decade, we compute spatial averages over all the background stations and select the days with a mean PM_{10} above 80 µg m^{-3}. Even though the network of ground-based stations is designed to be the most representative of the regional air quality, the spatial resolution remains coarse and the average could be not representative of all areas of the Paris region.

20   Figure 2 gives the histogram for APEs exceeding the information threshold during the eleven winters from 2007/2008 to 2017/2018. The light (dark) colours represent the occurrence of days with at least one station exceeding 50 µg m^{-3} (80 µg m^{-3}). Such a selection yields an overview of polluted days in winter during the last decade. Among these eleven winters (Figure 2), we count 136 (27) days with at least one station exceeding the information (alert) threshold. Figure 2 also shows a slight improvement of the air quality in the Paris metropolitan area in winter over the last decade. The frequency of pollution

25   threshold overruns tends to decrease over the years. Yet, winter 2016/2017 stands out with a large number of threshold exceedances, in opposite to the previous and following winters, i.e. 2015/2016 and 2017/2018, that present few threshold exceedances. This multi-annual variability is related with the prevailing meteorological conditions, namely the occurrence of strong and persisting anticyclonic situations. Indeed, despite a general trend in emissions to decline in the Paris region, there are still noteworthy episodes of pollution. When a strong high pressure system sets in over a long period of time, it prevents

30   air mass advection, blocking the weather situation. Thus, the pollution still emitted, even if it is less than in the past, remains

blocked by the high pressure system and ends up exceeding the health thresholds (Menut et al., 1999a; Vautard et al., 2003; Chazette and Royer, 2017).

When considering the spatial averaging, 8 days of aerosol pollution are highlighted, split into the four different episodes presented in Table 2. The first two episodes (during winter 2007/2008 and winter 2008/2009) seem to have been the most severe: each time, the daily spatial average surpassed 110 µg m^{-3} in Metropolitan Paris during two consecutive days. During the winter of 2016/2017, we count two extremely polluted days belonging to two distinct APEs. Both are sampled by the ground-based lidar. As will be presented in Section 4, they share significant AEC levels and shallow PBLs. The first event begins on 30 November 2016 and ends on 2 December late in the evening. The second event takes place in January 2017: it begins on 20 January and ends during the night of 23-24 January, with a peak on 22^n January. According to ERA5 reanalyses, the meteorological patterns (see section 3.2) are similar over the 8 days: surface pressure above 1015 hPa, temperature close to 0°C, relative humidity around 80% and very low wind speed (< 3 m s^{-1}) within the PBL (Table 2).
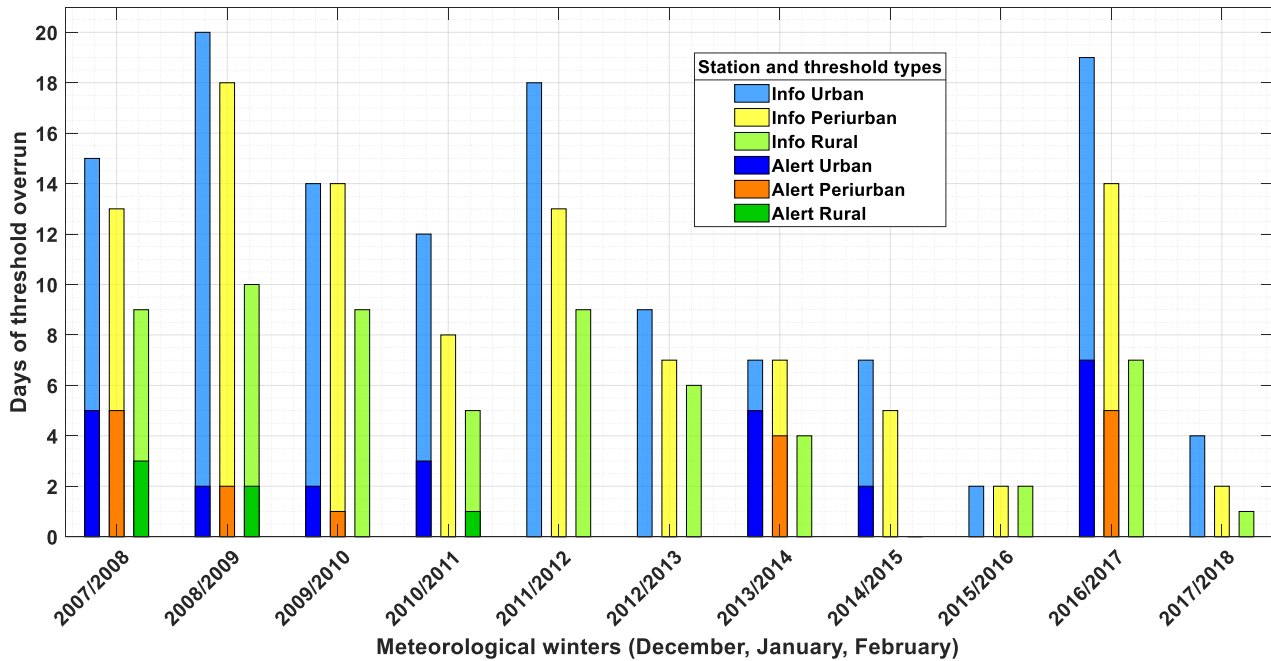
Figure 2: Diagram representing the number of days comprising at least one station where a threshold is exceeded (light colours for information and dark colours for alert) for each winter of the past decade. The stations taken into account are only background ones. The station typing (urban [light / deep blue], suburban [yellow / orange] and rural [light / deep green]) is conserved to appreciate the spatial extent of a typical polluted day.

Table 2: The 8 most severely polluted winter days of the past decade. For each day we give both PM$_{2.5}$ and PM$_{10}$ measured at ground level (Airparif network) in the format Max/Mean/Min where: Max and Min are the hourly maximum and minimum value measured at a given background station during the day and Mean is the daily average over all background stations. Meteorological parameters

(ECMWF ERA5) at ground-level are also given: pressure (P), temperature (T), relative humidity (RH), wind speed (WS) and wind direction (WD) with the standard deviation associated to the daily average.

Winter	2007/2008				2008/2009		2016/2017	
Date	21 Dec	22 Dec	23 Dec	24 Dec	10 Jan	11 Jan	1 Dec	22 Jan
PM_{10} ($\mu g\,m^{-3}$)	151/82/35	204/88/26	215/131/86	182/121/58	223/111/60	238/123/68	241/97/24	171/82/39
$PM_{2.5}$ ($\mu g\,m^{-3}$)	-	-	-	-	176/100/54	208/120/55	159/64/19	156/64/32
P (hPa)	1016±1	1015±1	1018±1	1017±1	1017±1	1019±1	1019±2	1015±1
T (°C)	-1.7±3.2	-0.8±3.5	0.1±3.2	-0.7±3.5	-6.9±3.5	-3.8±4.8	-0.7±3.5	-3.2±3.4
RH (%)	83±9	81±9	85±9	87±9	86±8	82±12	84±11	83±9
WS ($m\,s^{-1}$)	2.3±0.2	2.1±0.4	1.3±0.8	2.2±0.6	1.4±0.8	2.8±0.5	1.6±0.8	1.8±0.4
WD (°)	126±10	155±22	217±97	180±12	140±92	180±8	274±27	99±15

3.2 Favourable weather conditions

Over the Paris area, APEs occur when weather conditions favour northeast advection in the lower and middle troposphere towards the Ile-de-France region (e.g. Chazette and Royer, 2017), or in presence of a weather-blocking situation (e.g. Menut et al., 1999; Bessagnet et al., 2005; Petit et al., 2017), particularly in winter.

3.2.1 Synoptic situation

The analysis of large-scale meteorological patterns before and during each of the four afore mentioned events helps to understand how a severe APE can settle in. The common denominator is the perturbation of the usual oceanic wind regime by a high-pressure system. APEs of 2007, 2009 and 2017 share a similar establishment process: a high-pressure system descending from high latitudes blows air from Eastern Europe and settles above Central Europe during a few days. While this meteorological episode lasts, the Azores anticyclone combines with the existing high in central Europe to form a vast high-pressure system with very little wind, as shown in Figure 3b. A low-pressure system coming from the South for 2009 and 2017, or the West for 2007, finally weakens the high and ends meteorological conditions favourable to an APE.

Figure 3a shows the weather situation that occurred in early December 2016 at the 975-hPa level (within the PBL). It slightly differs from the other three major APEs in terms of location and orientation of its high-pressure system. Centred between Ireland and England, this transient but strong anticyclone blocks air masses of the Paris area and more broadly Northern France and Southern England, thus nullifying winds. During the night from 2 to 3 December, the deep low off the cost of Portugal weakens the high, making it go back to high latitudes. Located at the edge of the remaining high, the Paris area is seeing the return of winds and a dilution of its air pollution after 3 December 2016.
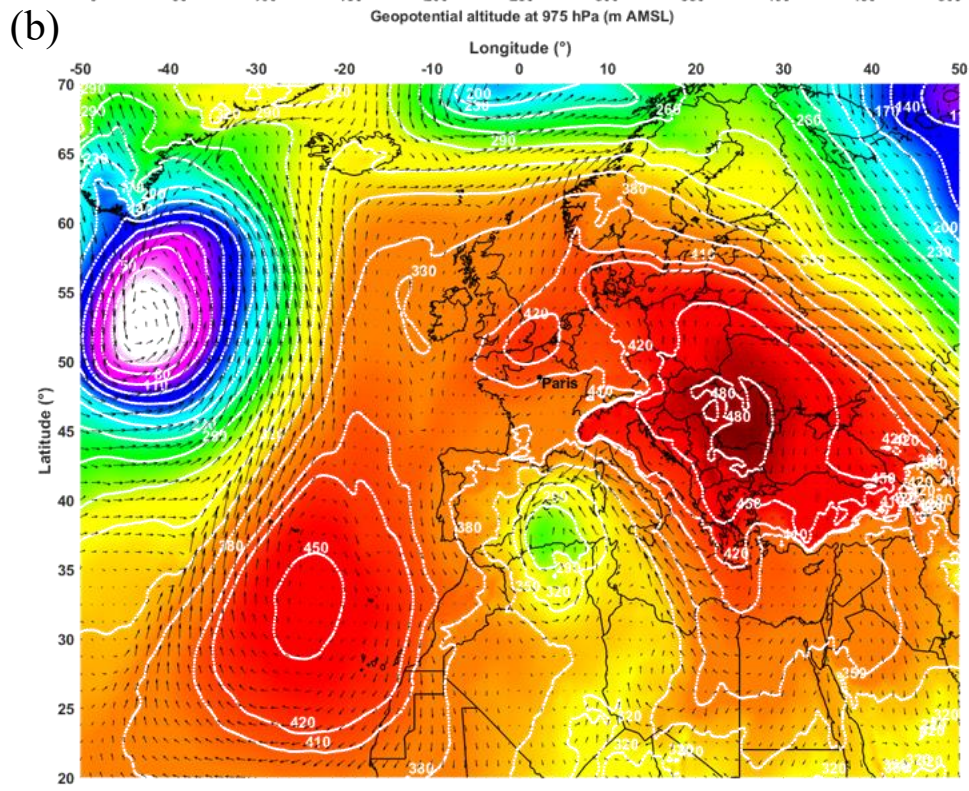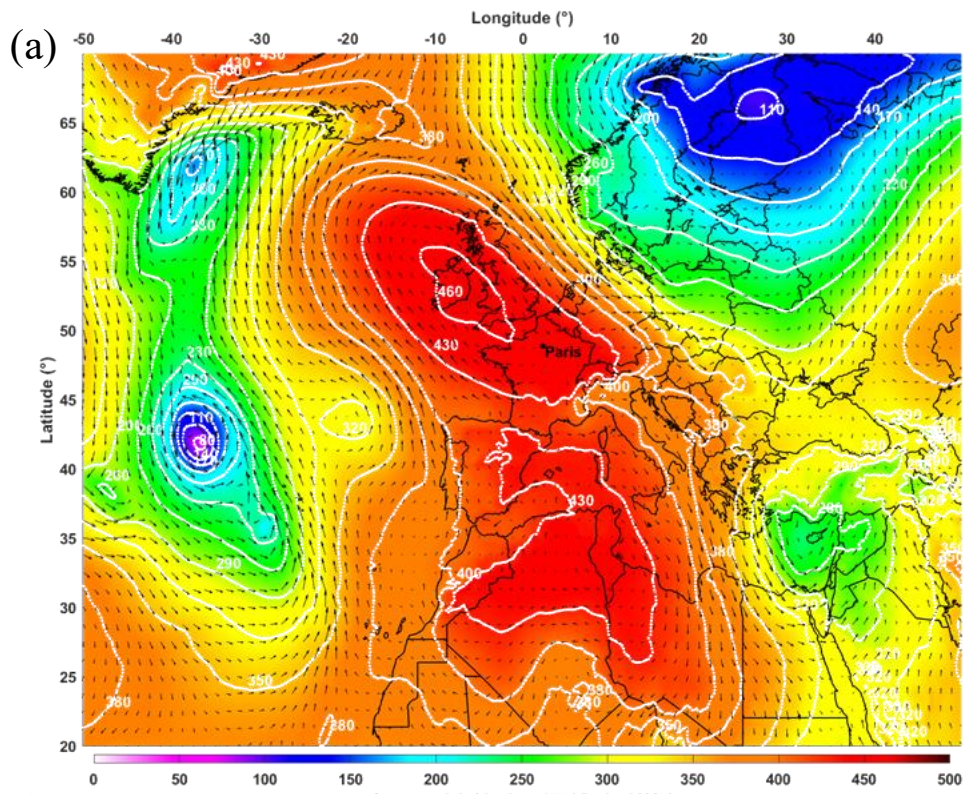
Figure 3: (a) Weather situation on 1 December 2016 at 12:00 UTC and (b) on 22 January 2017 at 12:00 UTC taken from ECMWF ERA-5 reanalysis. The geopotential altitude (white lines) and the wind direction and velocity (black arrows) are given at a 975-hPa level. Maximum wind speed is 27.8 m s^{-1} (31.6 m s^{-1}) at 57.75°N 28.25°W (62.25°N 39.5°W) on the top (bottom) map. Minimum wind speed is 0.02 m s^{-1} (0.03 m s^{-1}) at 50.5°N 6.5°E (46.25°N 7.75°E) on the top (bottom) map.

3.2.2 Local winds

At ground level, ERA5 reanalyses from ECMWF show how wind patterns behave in Paris during an APE. We consider the single grid point of 0.25° x 0.25° which includes central Paris (48.875°N, 2.375°E). Figure 4 displays the hourly wind speed of the four days comprising the APE of December 2016. We note that two days before the event (28 and 29 November), winds are above 4 m s^{-1} and coming from the northeast (Figure 4), whereas for the two polluted days on 30 November and 1 December, winds remain below 3 m s^{-1} and have no privileged direction.

Likewise, for the three cases of 2007 (a), 2009 (b) and 2017(c), whose wind roses at ground-level are shown in Figure 5, winds are stronger on days before PM levels rise, and remain below 3 m s^{-1} when high aerosol concentrations are observed. Each time, the establishment of the high-pressure system brings in air masses from the East (a), or North-East (b and c). Once settled above Central Europe, between 45°N and 50°N, the high largely weakens wind speed (c) or completely nullifies it (a and b).

We note that in the case of January 2017, winds keep a privileged direction according to reanalyses, as the Paris region remains at the edge of the high. Still, those winds from the North-East do not permit any dilution of an aerosol load covering Northern France, Benelux and Western Germany, as shown by ensemble reanalyses of chemical transport models available on the CAMS website (https://atmosphere.copernicus.eu/).
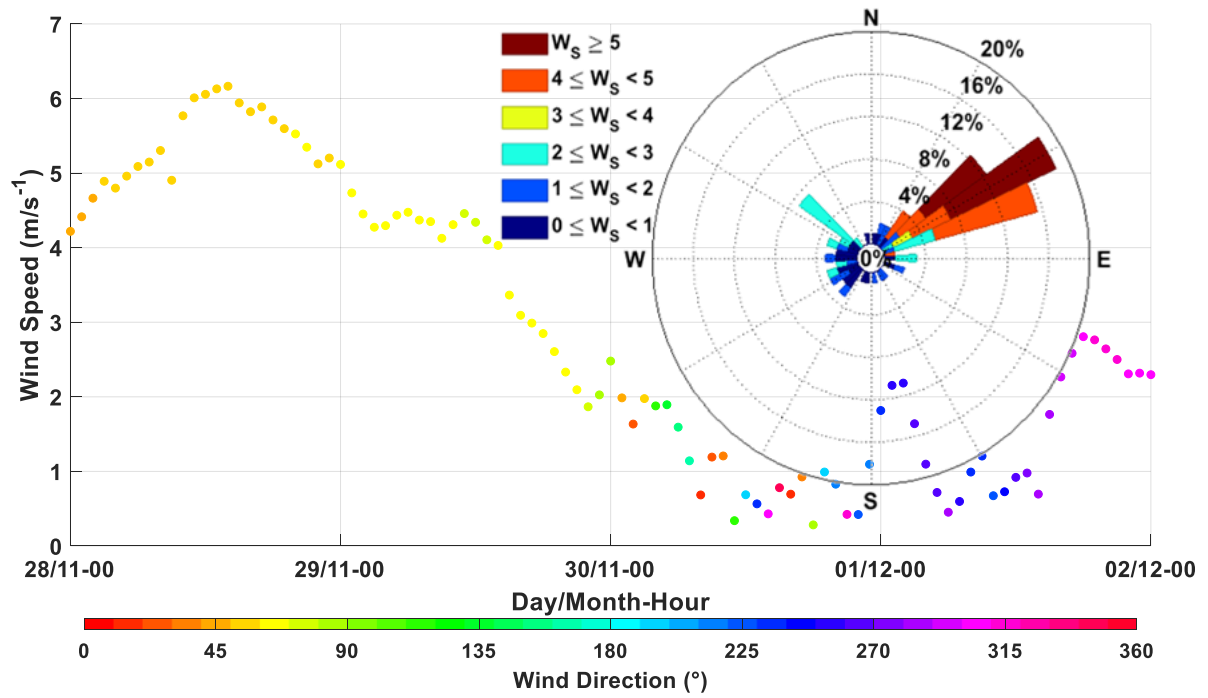
Figure 4: Wind rose and temporal evolution of wind intensity and direction at 10 m from ERA5 during four days of the 2016 APE. The coloured scale for wind speed (Ws) refers to the windrose.
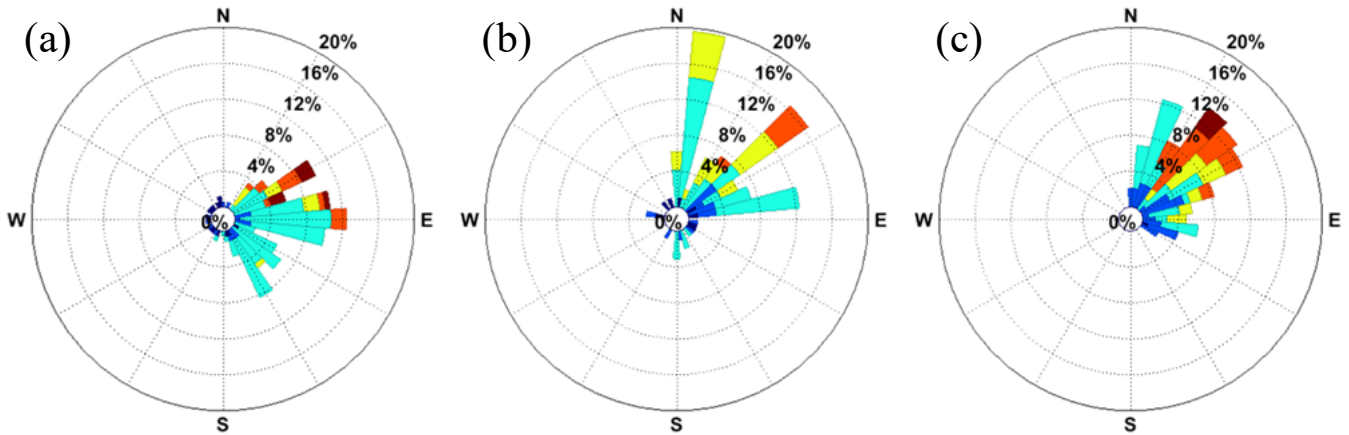
5   **Figure 5: Wind roses compiling ERA5 data for 7 (a), 4 (b) and 6 (c) days respectively for the 2007, 2009 and 2017 pollution episodes. The colour code is the same as in Figure 4.**

4 Lidar-derived aerosol optical properties

4.1 AEC and AOT

Figure 6 shows the temporal evolution of the vertical profiles of the AEC during the two pollution events. The AEC is a good proxy for the aerosol load found in the atmospheric column. As shown in Figure 6a, before 30 November, the sky is rather

5 aerosol-free and the PBL height reaches approximatively 700 m above ground-level (AGL) with AEC lower than 0.3 km^{-1}. From 30 November, the AEC significantly increases with a maximum value close to 0.5 km^{-1}. In the evening and the following night, aerosols are trapped within the first 400 m AGL and the AEC reaches values close to 1 km^{-1} at 12:00 UTC on 1 December. The PBL remains constrained to 400±50 m AGL until the end of the pollution event on 2nd December.

Figure 6b shows a sharp variation of the PBL top between 21 and 22 January, where it decreases from 700 to less than 300 m

10 AGL. This decrease is closely linked to the installation of an anticyclonic system over most of Western Europe (see Section 3.2). The AEC remains of the same order of magnitude as during the first pollution event. The two pollution events share a drastic PBL thickness abatement and high AEC values, but the first event appears more suddenly.

The lidar-derived AOT (AOT$_{lid}$) is obtained at 355 nm by integrating the AEC profiles, while the AERONET-derived AOT (AOT$_{phot}$) is computed from AOT$_{phot}$ at 440 nm to 355 nm using the Ångström law (Ångström, 1964). As shown in Figure 7a

15 and Figure 8a, the lidar-derived AOT matches the sun-photometer-derived AOT except for 1 December (Figure 7a) and 21-22 January (Figure 8b). These discrepancies are mainly due to the presence of middle and high-altitude clouds identified on lidar vertical profiles (white bands in figures 6b and 8a), which may bias the AERONET operational products (Chew et al., 2011). As far as lidar data are not disturbed these profiles are kept in the figure. For the two winter pollution events of 2016/2017, the AOT at 355 nm remains below 0.5. Note that for 1 December 2016 (22 January 2017), when comparing the MODIS-derived

20 AOT at 550 nm of 0.12±0.07 (0.15±0.07) with the AOT$_{phot}$ of 0.16±0.06 (0.11±0.03) at the same wavelength, their difference of 0.04 is within the error bars. All the available values of AOT are summarized in Table 3. For early events in the decade, cloud cover made the availability of AERONET and MODIS level 2 products very rare; only one value from MODIS on 22 December 2007 with AOT = 0.16±0.07 is available. An example of the AOT field as derived from MODIS is given in Figure 9 on 21 January 2017. This highlights the horizontal extent of the pollution plume when observations are not contaminated by

25 clouds. The AOT field appears to be homogeneous within its spatial extension. It is therefore likely that the conclusions deduced from the observations on Paris city may be generalized to a larger spatial scale.
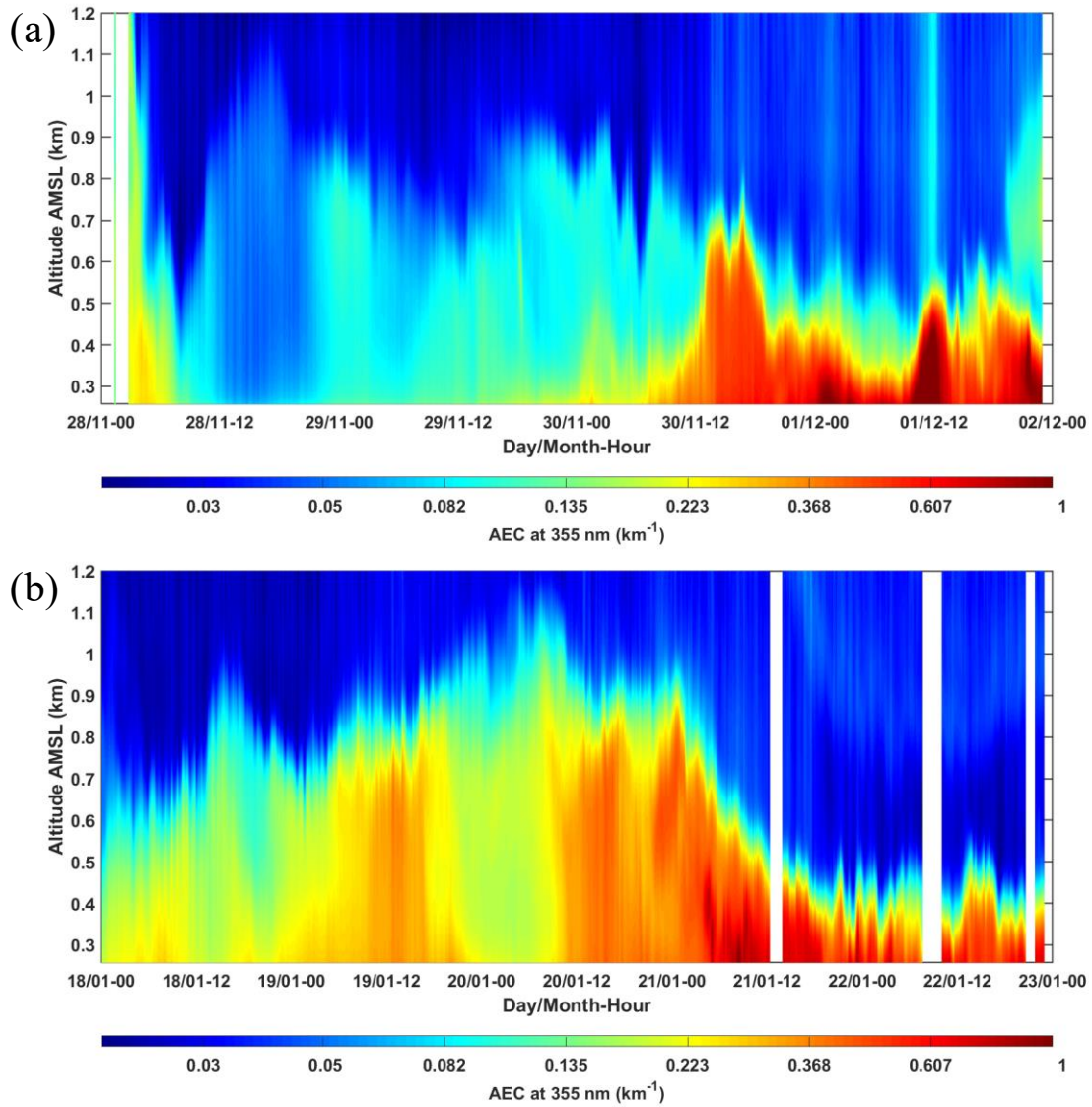
Figure 6: Temporal evolution of the aerosol extinction coefficient (AEC) at 355 nm as a function of time and altitude for the two cases discussed (a) in late 2016 and b) in January 2017. The colour set from blue to dark red shows an AEC from almost 0 to above 0.6 km⁻¹. White stripes correspond to the presence of clouds.

4.2 Lidar Ratio

It is well established that the LR varies with the types of aerosols present in the atmospheric column (Müller et al., 2007; Omar et al., 2009; Amiridis et al., 2011; Chazette et al., 2016;). Figure 7a and Figure 8a show the temporal evolution of LR derived from the N_2-Raman ground-based lidar for the two APEs of the winter of 2016/2017.

The LR is quite variable for the December APE, with values ranging from ~30 to ~90 sr and a mean value of 59±18 sr. This temporal variation trace a diurnal evolution with smaller particle size during night time, as highlighted in Figure 7b, when the $PM_{2.5}$ to PM_{10} ratio slightly increases during the night (e.g. from 0.4 to 0.6 during the first night, 28 November). This increase may be explained by the diurnal variation of aerosol production in an urban area (Airparif, 2014). Indeed, mechanical processes

5   inducing abrasion (tires, breaks …) linked to human activity and resuspension processes, which are the main source of coarse particles with aerodynamic diameters larger than 2.5 µm, decrease during the night. Resuspension during daytime was highlighted as a possible cause of discrepancies between model and observation during the ESQUIF project in the Paris surroundings (Hodzic et al., 2004, 2006). This could be the underlying cause of the diurnal variations of both the LR and the $PM_{2.5}$ to PM_{10} ratio. The fine fraction of AOT given by the AERONET operational product is also plotted in Figure 7b

10   (available only during daytime). It agrees with an increase of LR when the load of smaller particle increases from one day to the next.

For the APE in January, the LR is pretty much constant over time, ranging between 40 and 50 sr, with a mean value of 45±7 sr (Figure 8a). This period is associated with almost constant values of the fine fraction of aerosol (94±2%) and a ratio of $PM_{2.5}/PM_{10}$ of 0.77±0.06 (Figure 8b).

15   When only the most polluted days are considered, i.e. 1 December and 22 January, the LR increases to 74±16 sr and 56±15 sr, respectively. The presence of smaller particles may be suspected during the first pollution event (sun-photometer-derived visible Ångström exponent of 1.5±0.1 compared to 1.1±0.3 for the second event, see Table 3), likely due to specific meteorological circulation (see Section 3.2) and the presence of younger aerosols. LPDR also corroborate this assumption (Table 3) with higher values in December than in January, whether it is from CALIOP data at 532 nm (9% versus 6%) or the

20   ground-based lidar data at 355 nm (10% versus 5%).

Figure 9 shows the CALIOP and CATS ground-tracks for the January APE. Within a 24-hour time interval, their tracks are crossing in the middle of France, along a south-north axis for CALIOP and a west-east axis for CATS. The distances between the ground-based lidar and the spaceborne lidars ground-tracks are substantial (~200km for CATS, the farthest track). However, according to ensemble reanalyses of chemical transport models available on the CAMS website

25   (https://atmosphere.copernicus.eu/) and given the meteorological conditions discussed above, the pollution plume seen by MODIS (AOT > 0.1 in light blue South of Paris) seems to originate from the spreading of the urban haze. The distance separating the ground-based lidar and the farthest ground-track is inferior to the characteristic size of the dispersed plume. Thus, it can be assumed that the spaceborne and ground-based lidars measured the same type of aerosol and that their data are comparable.

30   For the nocturnal orbit on 30 November - 1 December, the CATS operational product types aerosols as "Polluted continental" corresponding to a LR of 65 sr at 532 nm (see Figure 8a). For the following night, the LR set by CALIOP is 70±25 sr, corresponding to "Polluted continental / smoke" aerosol type, which is coherent with the CATS operational product (Table 3). The LR given by the two spaceborne lidars matches the values derived from the ground-based lidar, although it is not the same wavelength. Note that Müller et al. (2007) show that the difference on the LR between 355 and 532 nm is in the range of 10%

for urban haze aerosols. Our results are consistent with the ones of these authors for urban haze in Central Europe and North America showing lidar-derived LR at 355 nm of 58±12 sr and 53±10 sr, respectively. The aerosol typing derived from CATS at 03:00 UTC on 20 January and CALIOP at 02:00 UTC on 21 January is identical to the one previously retrieved for the event of December (Table 3, Figure 7a) although the LR retrieved from the ground-based lidar decreases. Such a discrepancy is not significant when considering the expected uncertainty on the LR given by CALIOP (25 sr).
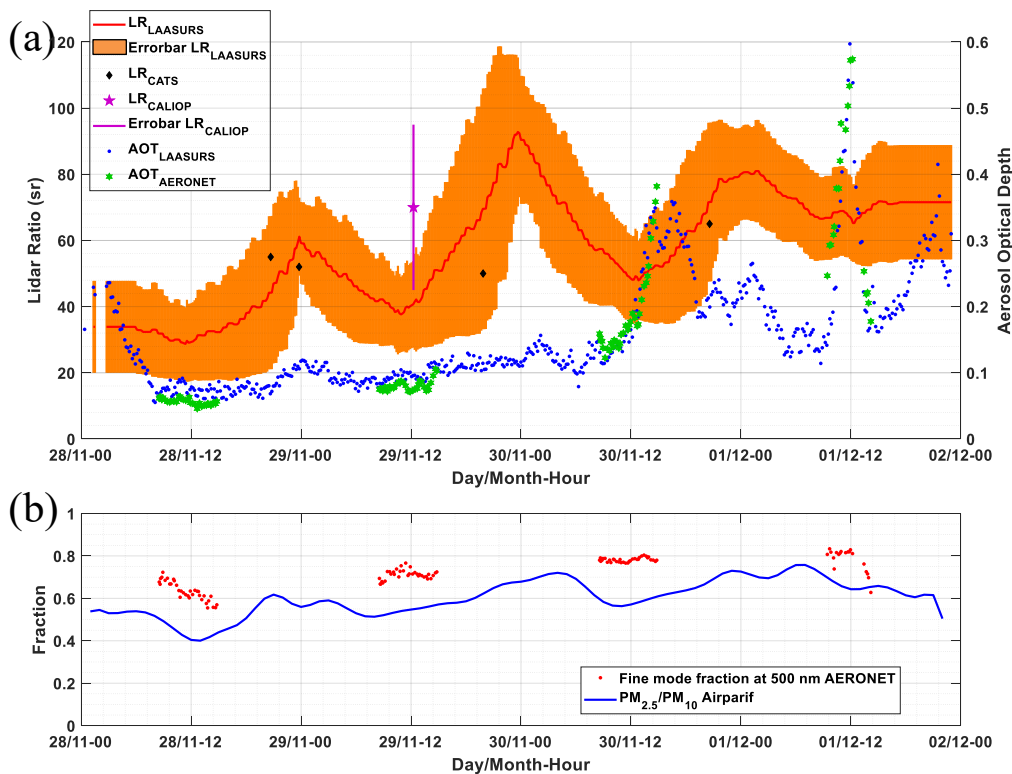
Figure 7: (a) Time series of Lidar Ratio (LR) and AOT at 355 nm on November-December 2016. On the left Y-axis, the LR as retrieved from lidar measurements is presented in red. The orange area is the associated standard deviation. The LRs extracted from CATS and CALIOP operational products are represented as black diamonds and a purple star, respectively. On the right Y-axis, AOTs at 355 nm retrieved from LAASURS and AERONET are represented in blue and green. (b) The temporal evolution of the fine mode fraction operational product from AERONET is plotted along the PM2.5 to PM10 ratio from Airparif measurements.
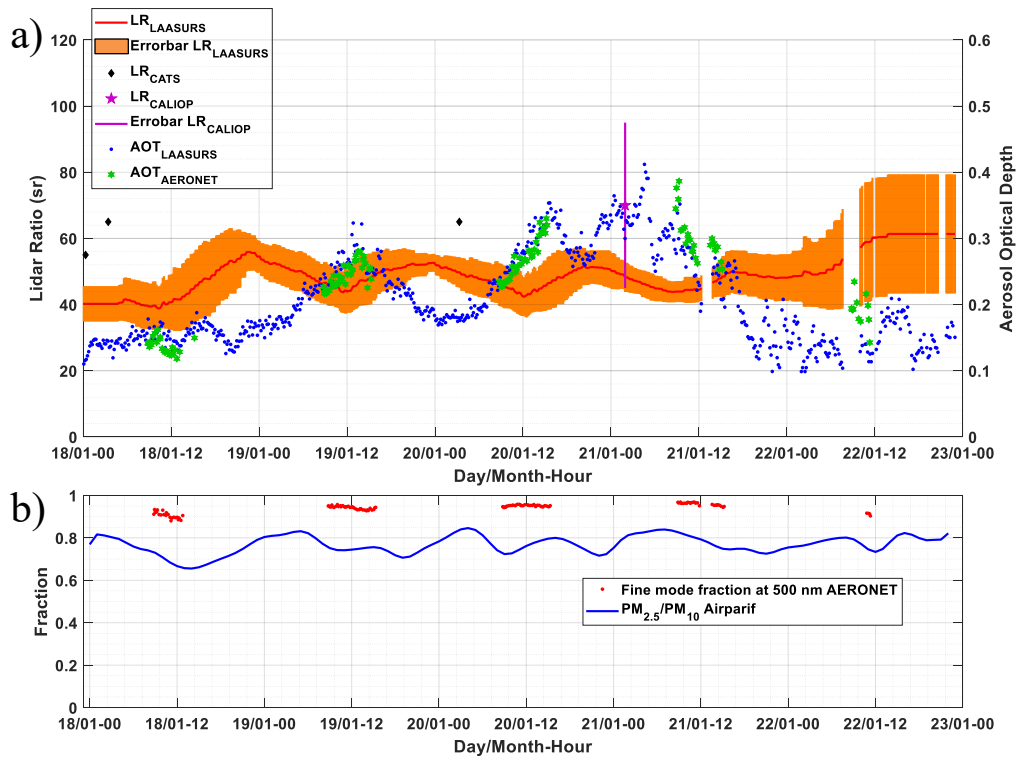
Figure 8: Same as Figure 7 but for the January 2017 pollution event
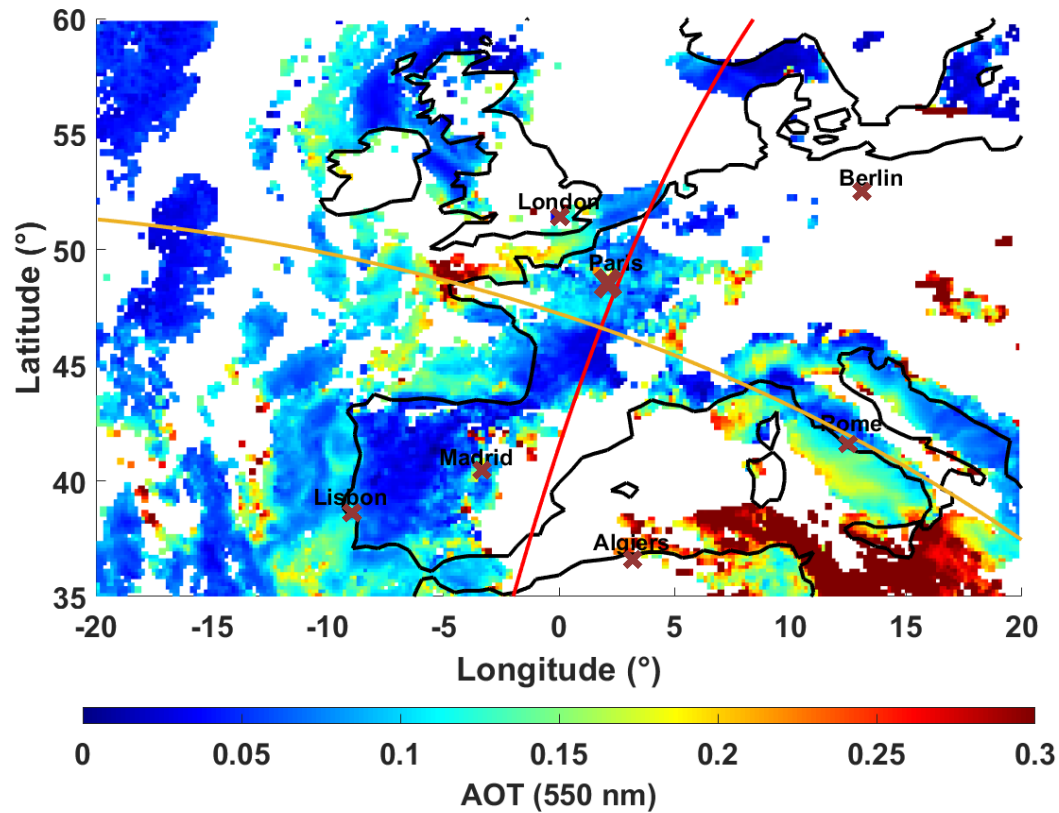
Figure 9: MODIS-derived aerosol optical thickness (AOT) at 550 nm on 21 January 2017. Red and orange solid lines, respectively show the ground-tracks of CALIPSO/CALIOP (03:19 UTC 20 January) and ISS/CATS (02:10 UTC 21 January).

Table 3: Optical properties encountered during the two most polluted days of the winter 2016/2017.

	Date	2016 APE	2017 APE
AOT	**AERONET** 355 nm 550 nm	0.32±0.1	0.18±0.02
		0.16±0.06	0.11±0.03
	MODIS 550 nm	0.12±0.07	0.15±0.07
	LAASURS 355 nm	0.23±0.09	0.15±0.03
å	**AERONET** 340 nm 675 nm	1.5±0.1	1.1±0.3
LR (sr)	**CALIOP** 532 nm	70±25[1]	70±25[3]
	CATS 532 nm	65[2]	65[4]
	LAASURS 355 nm	72±15	56±15
LPDR	**CALIOP** 532 nm	0.09[2]	0.06[3]
	LAASURS 355 nm	0.10±0.03	0.05±0.02

5 In situ ground-based measurements versus lidar inversed data

5.1 PM_{10} and $PM_{2.5}$ at ground-level

The temporal evolutions of surface PM during the two particulate pollution events of winter 2016-2017 are analysed. Figure 10 displays both $PM_{2.5}$ and PM_{10} during the APEs of December 2016 and January 2017. Only the background stations (BS) are taken into account. For PM_{10} and $PM_{2.5}$, an hourly average is calculated over all these stations in the Paris vicinity. The related standard deviation surrounds each mean value of PM (coloured area). The information and alert thresholds are also represented.

Figure 10a shows a continuous increase of both $PM_{2.5}$ and PM_{10} from 29 November to 2 December. The information threshold of 50 µg m^{-3} for PM_{10} is exceeded around noon on 30 November. The aerosol mass concentrations overtake the alert threshold of 80 µg m^{-3} for PM_{10} during the night of 30 November – 1 December as the PBL top height decreases. PM_{10} averaged over the Paris region reaches 121 µgm^{-3} on 1 December, just as the lidar records a significant enhancement of the AEC in the entire PBL. Figure 10b shows PM_{10} values around 30 µg m^{-3} during the first days, except at the end of 19 January, when the information threshold is exceeded. A significant decrease of the PBL top height occurred on 21 January at nightfall; preventing the dilution of aerosol, it leads to a strong increase of PM_{10}. Indeed, as seen in Figure 6b, the PBL height is halved during 21 January when PM_{10} doubles. The standard deviation of both $PM_{2.5}$ and PM_{10} are larger on 30 November and 1 and 2 December 2016 than on 20, 21 and 22 January 2017. It indicates a greater geographical variability of the pollution plume during the first APE of December. This suggests that PMs are more sensitive to local aerosol sources for the December event than for the one of January.
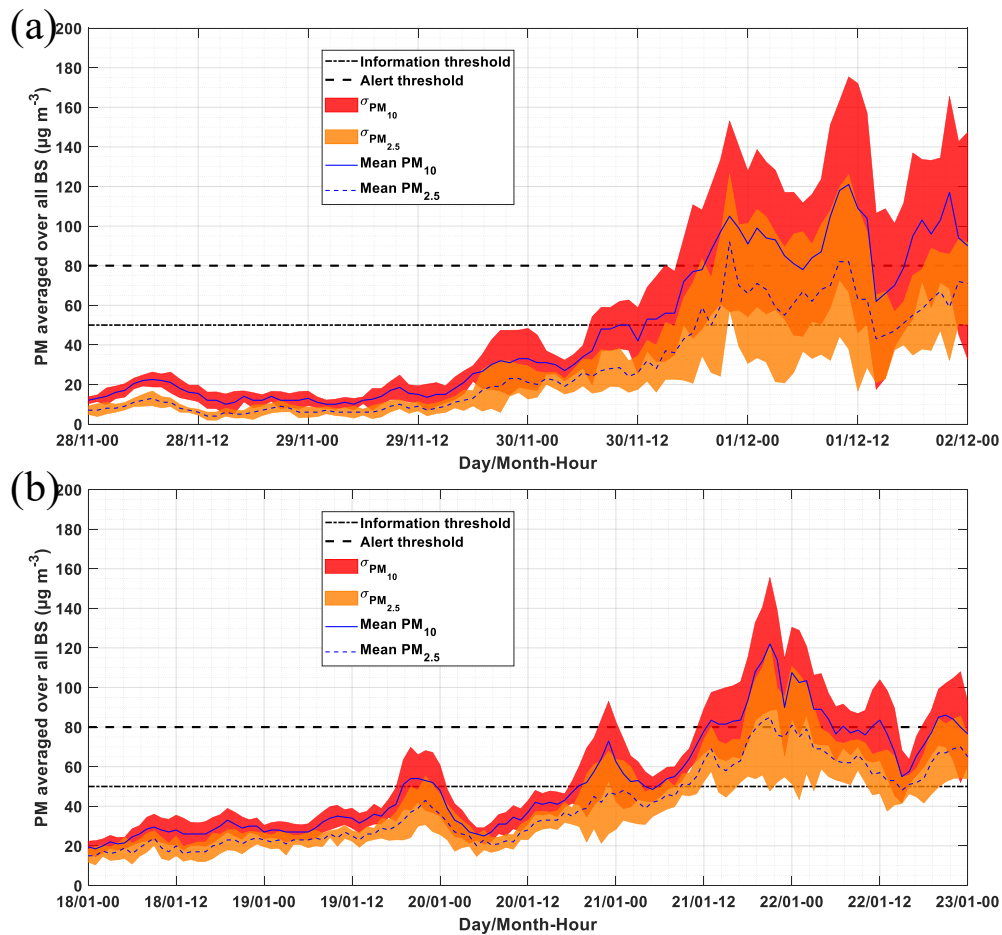
Figure 10: Temporal evolution of hourly ground PM$_{2.5}$ and PM$_{10}$ during the aerosol pollution events of (a) December 2016 and (b) January 2017. The lines are averages over all the background stations (BS) of Ile-de-France, respectively for PM$_{2.5}$ and PM$_{10}$; the coloured areas highlight the standard deviations.

5.2 Relationship between aerosol optical properties and PM$_{2.5}$

The parameter legally used to gage an APE is PM$_{10}$ (n° 2008/50/CE and 2004/107/CE), however, Randriamiarisoa et al. (2006) demonstrate that the accumulation mode (PM$_{2.5}$) contributes the most to optical properties of an aerosol population in the Paris area. Thus, in search of a correlation between Figure 6 and Figure 10, we chose PM$_{2.5}$ over PM$_{10}$. We consider the dataset combining the two events displayed in Figure 6, Figure 7 and Figure 10. It ranges from pollution free days to severely polluted days and thus covers a wide range of AEC, AOT and PM$_{2.5}$ values.

5.2.1 Integrated optical properties

Erreur ! Source du renvoi introuvable. shows the scatterplot between the PM$_{2.5}$ measured at ground level and the total AOT$_{lid}$. The linear regression conducted on all data of **Erreur ! Source du renvoi introuvable.** (dashed grey line), i.e. AOT

and PM$_{2.5}$ day and night for the two pollution episodes sampled by lidar, shows no correlation, with a Pearson correlation coefficient R² ≈ 0.16. However, a group of points stands out from this dataset and is associated with a PBL top below 600 m AMSL. It appears that most of these points are also associated with PM$_{2.5}$ values above the information threshold (50 µg m^{-3}). The linear regression conducted without this set of points (black solid line of **Erreur ! Source du renvoi introuvable.**) shows a better correlation (R² ≈ 0.66). It suggests that the direct correlation between AOT and PM$_{2.5}$ to assess air quality, as proposed by Wang and Christopher (2003), Gupta et al. (2006) and Kacenelenbogen (2006), cannot be used under low PBL height conditions. Scatterplots (not shown) made with PM$_{10}$ instead of PM$_{2.5}$ show even worse correlation (R² ≈ 0.03 and R² ≈ 0.61, respectively). Indeed, correlating ground-level measurements with the atmospheric columnar properties can be difficult. In the case of winter pollution, the PBL dynamic does not argue in favour of such an approach: very low surface temperatures (~0°C) lead to very high stability in the PBL and prevent the convection processes. The surface layer is therefore uncorrelated with the rest of the PBL. One obvious consequence is that a diminution of the PBL top height will be reflected in the PM values at the surface but not necessary in the measured AOT. This dichotomy is even more obvious with the free troposphere, whose exchanges are very limited by the inversion layer. It should also be noted that relative humidity is often highest at the top of the boundary layer and may induce, depending on the hygroscopic properties of the aerosols, a significant increase in AOT that is not related to the PM$_{2.5}$ values at the ground level (Chazette et al., 2005).

In **Erreur ! Source du renvoi introuvable.** the AOT is divided by the PBL height derived from the lidar profiles as in Menut et al. (1999), estimating a column-average AEC in the PBL. This technique is used to improve the correlation in Koelemeijer et al. (2006) but can be applied only when the aerosol load in the free troposphere is assumed negligible. We find a significant improvement with the Pearson correlation coefficient rising to ~0.61. This AOT to PBL height ratio is clearly a better proxy to assess the ground-level aerosol concentration from the AOT but the presence of an aerosol layer above the PBL limits its use.
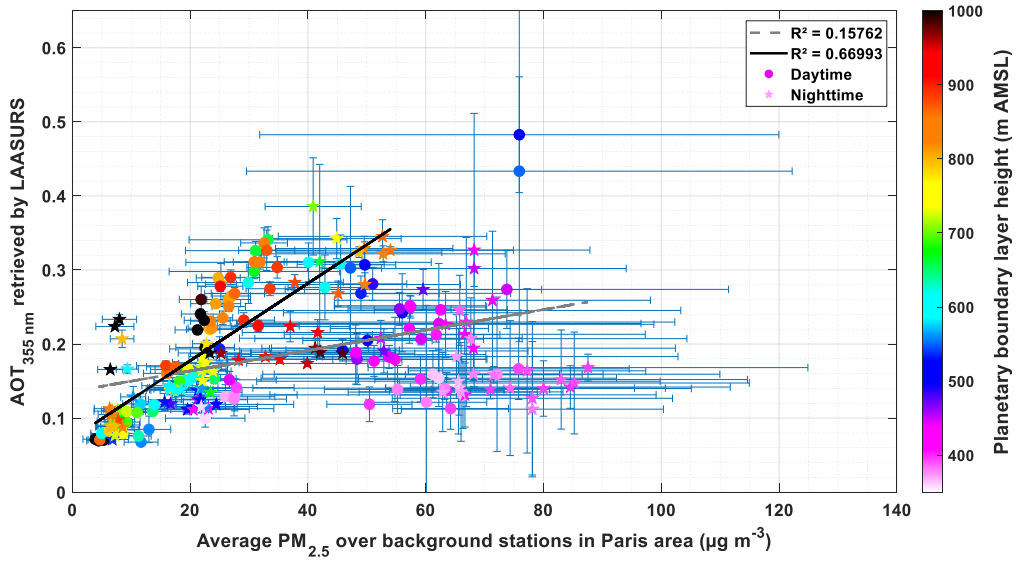
Figure 11: Relationship between PM$_{2.5}$ (X-axis) and Aerosol Optical Thickness retrieved by lidar at 355 nm (AOT$_{lid}$) (Y-axis) for the dataset presented in Figure 7 and Figure 10 overlapped. The colour set indicates the PBL height retrieved by lidar for each point. Error bars represent the standard deviations due to time average (AOT$_{lid}$) and spatial average (PM$_{2.5}$). The daytime (nighttime) data are represented by discs (stars). The grey dashed line (black solid line) illustrates the linear regression computed from all the trend lines (the set of points associated with a PBL top above 600m AMSL). The correlation coefficients can be found in the top right-hand corner.
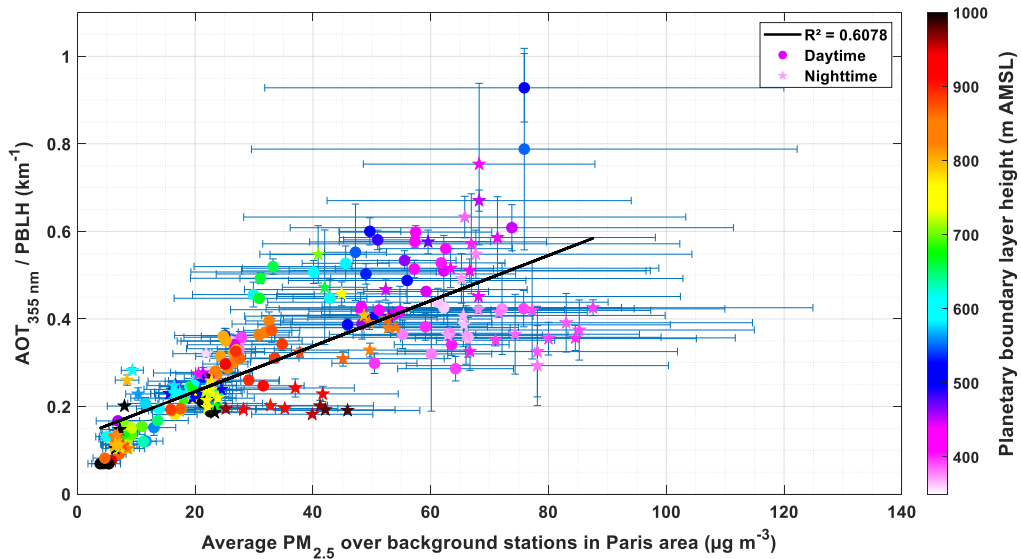
Figure 12: As Erreur ! Source du renvoi introuvable. but dividing AOT$_{lid}$ by the boundary layer height (BLH) in Y-axis.

5.2.2 Lidar-derived aerosol extinction coefficient

Another proxy appreciating the intensity of the aerosol load within the PBL would be the maximum of the lidar-derived AEC (AEC_{max}) within the PBL. Figure 13 shows the scatterplot of the AEC_{max} against $PM_{2.5}$ for the APEs. We find a significant linear relation with a Pearson correlation coefficient of ~0.75. Here, the average altitude where the AEC_{max} is found is ~300±90 m AMSL (~200±90 m AGL). In a stable PBL with barely any wind shear, AEC_{max} is close to the ground and its variations are comparable to the ones observed on $PM_{2.5}$. Hence, this optical parameter appears as the most appropriate to monitor the evolution of ground-level winter particulate pollution using ground-based lidar measurements, whether it is heavily polluted or not. Compared with the previous method, the presence of aerosols in the free troposphere does not bias the linear relationship established. However, this approach should not be generalized too quickly for well-developed PBLs that may have high relative humidity at their top. In the case of hydrophilic aerosols, as is often the case for Paris pollution aerosols (Randriamiarisoa et al., 2006), the AEC_{max} may be found near the top of the PBL. Note that at low winter temperatures, aerosols are generally less acidic and therefore less hydrophilic (Jaffrezo et al., 2005). Here we find 358±229 m as the averaged difference between PBL height and the altitude of AEC_{max} over all the available profiles. This mean distance is associated with a high standard deviation resulting from the high variation of the PBL height within the considered dataset (~640±250 m AMSL).
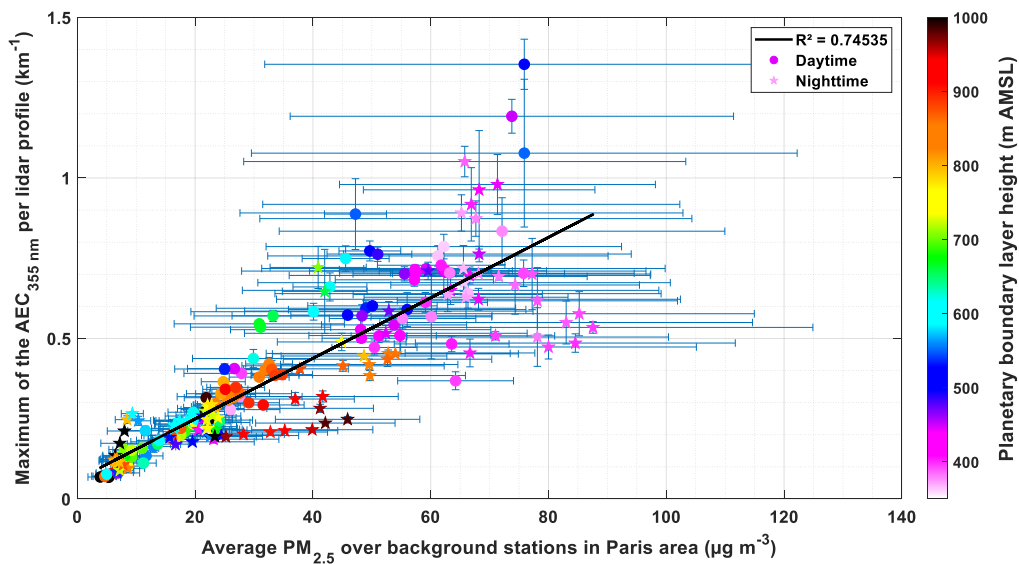
Figure 13: As Erreur ! Source du renvoi introuvable. **but replacing AOT$_{lid}$ by the maximum value of the AEC profile retrieved by the LAASURS within the PBL.**

5.3 Discussion

In Figure 14 a third independent dataset is added to test the relevance of the linear fit shown in Figure 13. As the dataset recorded during the two major APEs, this third dataset is also sampled during the WASLIP experiment. It covers eight days

from the 3 to 10 December 2016 and the data processing methodology is the same that the one used for the two major pollution events. This third period corresponds to an intermediate pollution situation with $PM_{2.5}$ between 20 and 60 μg m^{-3}, included in the range of the two other polluted periods ($PM_{2.5}$ from ~5 to 90 μg m^{-3}). Figure 14 shows that this new independent dataset fits pretty well in the 95% prediction interval of the Figure 13 linear regression. The Pearson correlation coefficient of the new

5 linear regression performed on this third dataset is $R^2 = 0.5$. Furthermore, the computation of a linear regression on all the points, including the new dataset, results in a significant Pearson correlation coefficient $R^2 = 0.67$.

Regarding the slopes, each linear regression shows equivalent steering coefficients. These slopes are highly dependent on the chemical composition of the aerosols as shown by Raut and Chazette (2007). They correspond to the mean specific cross-section of the sampled aerosols, which is highly variable and a function of the emission sources, but also of the aerosol ageing

10 processes within the atmospheric environment. Here a value of 9.4 m^2 g^{-1} is found for the two major pollution events and 9.3 m^2 g^{-1} when the computation is made on all data in Figure 14. These values are higher than what can be find in the literature and in particular comparatively to the results of Raut and Chazette (2009) (table 1, maximum of 7.1 m^2 g^{-1}) and their review in table 2. These higher values could be explained by the use of $PM_{2.5}$ in this study rather than PM_{10}, indeed, the same computation with PM_{10} for the dataset of major APEs leads to a specific extinction cross-section of 7.0 m^2 g^{-1}.

15 Furthermore, the y-intercepts are slightly different between the two datasets. An approach using remote sensing of aerosols with the choice of a good optical proxy can give an estimate of the surface pollution in terms of $PM_{2.5}$, but should be used with caution the because of the possible temporal variability in the nature of aerosols, especially between long-range pollution events and local pollution. The most promising approach is the direct assimilation of the raw lidar observation into a chemistry-transport model including measurement modelling (Wang et al., 2013, 2014).
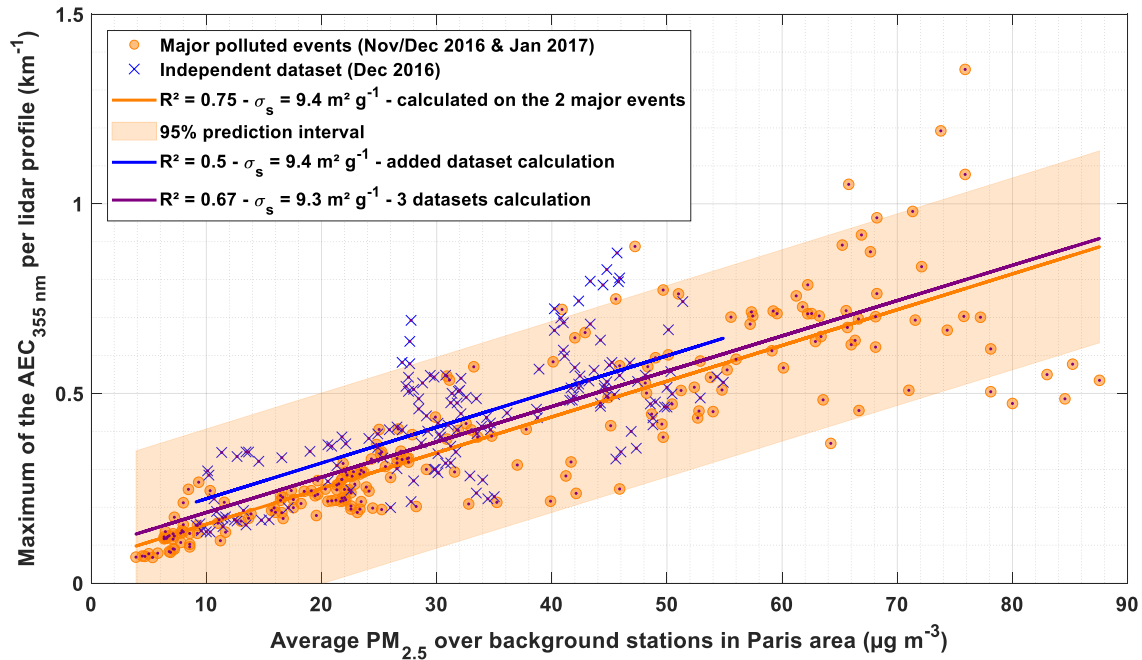
Figure 14: Relationship between PM$_{2.5}$ (X-axis) and AEC$_{max}$ within the PBL (Y-axis). Orange dots are the same dataset presented in Figure 13. Blue crosses are data sampled from the 5 to the 8 December 2016. The orange solid line corresponds to the linear regression computed from the orange points (same as Figure 13) and the light orange area illustrates its 95% confidence interval. The blue solid line is the result of the linear regression calculated on all the points (blue crosses and orange dots). The correlation coefficients can be found in the top left-hand corner.

6 Conclusion

In this paper the lidar-derived optical properties of two major APEs of the winter of 2016/2017, found to be part of the most severe pollution events of the 2007-2017 decade over Paris are investigated. This work is achieved through a synergy between: i) ground-based active and passive remote sensing devices, ii) spaceborne instruments, iii) air quality network measurements and iv) meteorological reanalyses. The data collected for this study highlight the maximum AEC in the PBL as an optical parameter that offers the possibility to assess the surface concentration of PM$_{2.5}$.

Although limited to a winter period, this lidar dataset comes to enrich the scientific literature, which was lacking severe winter pollution data. These episodes are rare (eight days in one decade, split between four separate events), but harmful for the citizens' health and still difficult to forecast. The two sampled APEs originate from different meteorological processes. The first is triggered by a high trapping local emissions around a small area which nullifies wind speeds. The other one is provoked by a strong widespread anticyclone blocking a large area during several days but with advection allowed by remaining winds at its edge. Furthermore, the suspected presence of younger and finer aerosol in the first APE is corroborated by the higher

values of both LR and LPDR retrieved during the aerosol pollution event of December (72 ± 15 sr and 10 ± 3 %, respectively) compared with the ones of January (56 ± 15 sr and 5 ± 2 %, respectively). In both cases, LR values are confirmed as "polluted continental" by spaceborne lidars and in accordance with the literature for urban haze.

Our results argue that in stable winter PBL conditions, no linear relationship exists between AOT and particle matter concentration at ground-level ($R^2\sim0.16$), i.e. a strong $PM_{2.5}$ at ground-level does not imply a significant AOT within the atmospheric column. This work shows a better agreement ($R^2\sim0.61$) when it comes to correlating the surface aerosol concentration with the PBL-averaged aerosol extinction coefficient (AOT to PBL top height ratio) and even better ($R^2\sim0.75$) with the maximum of aerosol extinction coefficient encountered within the PBL. The latter parameter shows a promising capability to monitor an APE during winter time, as it would not be affected by the aerosol presence above the PBL. Nevertheless, the established relationships are very dependent on the aerosol composition driving the specific extinction cross-section and a generalisation cannot be made without caution. Prior making a quantitative lidar derived PM-estimate using this technique, a reliable assessment of the specific extinction cross-section of the aerosol should be made (see Chazette et al., 2012a). Here the value found is 9.4 m^2 g^{-1} for $PM_{2.5}$ and 7.0 m^2 g^{-1} for PM_{10}. With a reliable tabulation of these cross-sections, spaceborne lidar aerosol products could transpose our approach from regional to global scale, albeit limited to sampling times corresponding to revisit of satellites. Future spaceborne lidar missions such as the ADM-Aeolus (Flamant et al., 2008) and the EarthCARE (Illingworth et al., 2015) satellites could expand the assessment of surface air pollution to a global scale in addition to in situ measurements.

Data availability. Data can be downloaded upon request from the first author of the paper.

Author contributions. Alexandre Baron wrote the paper et analysed the data. Patrick Chazette coordinated and performed the experiment, participated in the analysis and paper writing; Julien Totems performed the experiment and participated in the paper editing.

Competing interests. The authors declare that they have no conflict of interest.

Acknowledgements. This work was supported by the Commissariat à l'Energie Atomique et aux énergies alternatives (CEA). The Centre National d'Etude Spatial (CNES) helped maintain the Raman-lidar instrument. The authors would like to thank Pascal Genau (CNRS/LATMOS) and Cristelle Cailteau-Fischbach (UPMC/LATMOS) for their support in operating the lidar data and the welcoming on the QualAir station. François Dulac (CEA/LSCE) and the two unknown reviewers of this work are gratefully acknowledged for their constructive remarks, comments and suggestions during the review process of this work. The authors would like to thank the Airparif network for collecting data. The authors would like to thank the AERONET network for sunphotometer products (at https://aeronet.gsfc.nasa.gov/). The authors acknowledge the MODIS Science, Processing and Data Support Teams for producing and providing MODIS data (at https://modis.gsfc.nasa.gov/data/dataprod/),

the Atmospheric Science Data Center (ASDC) at NASA Langley Research Center (LaRC) for the data processing and distribution of CALIPSO products (level 4.20, at https://search.earthdata.nasa.gov/search) and CATS products (level 2, at https://search.earthdata.nasa.gov/search) . ECMWF data used in this study have been obtained from the Copernicus Climate Change Service Climate Data Store (https://cds.climate.copernicus.eu/cdsapp#!/home).

5   **References**

Airparif: Inventaire régional des émissions en Ile-de-France. Année de référence 2012 - éléments synthétiques, , 1–32, 2014.

Amiridis, V., Balis, D., Giannakaki, E., Kazadzis, S., Arola, A. and Gerasopoulos, E.: Characterization of the aerosol type using simultaneous measurements of the lidar ratio and estimations of the single scattering albedo, Atmos. Res., 101(1–2), 46–53, doi:10.1016/j.atmosres.2011.01.010, 2011.

10   Ångström, A.: The parameters of atmospheric turbidity, Tellus A, 16, 64–75, doi:10.3402/tellusa.v16i1.8885, 1964.

Ansmann, A., Riebesell, M. and Weitkamp, C.: Measurement of atmospheric aerosol extinction profiles with a Raman lidar, Opt. Lett., doi:10.1364/ol.15.000746, 2008.

Beekmann, M.: Monte Carlo uncertainty analysis of a regional-scale transport chemistry model constrained by measurements from the Atmospheric Pollution Over the Paris Area (ESQUIF) campaign, J. Geophys. Res., 108(D17), 8559,
15   doi:10.1029/2003JD003391, 2003.

Beekmann, M., Prévôt, A. S. H., Drewnick, F., Sciare, J., Pandis, S. N., Denier van der Gon, H. A. C., Crippa, M., Freutel, F., Poulain, L., Ghersi, V., Rodriguez, E., Beirle, S., Zotter, P., von der Weiden-Reinmüller, S.-L., Bressi, M., Fountoukis, C., Petetin, H., Szidat, S., Schneider, J., Rosso, A., El Haddad, I., Megaritis, A., Zhang, Q. J., Michoud, V., Slowik, J. G., Moukhtar, S., Kolmonen, P., Stohl, A., Eckhardt, S., Borbon, A., Gros, V., Marchand, N., Jaffrezo, J. L., Schwarzenboeck, A.,
20   Colomb, A., Wiedensohler, A., Borrmann, S., Lawrence, M., Baklanov, A. and Baltensperger, U.: In situ, satellite measurement and model evidence on the dominant regional contribution to fine particulate matter levels in the Paris megacity, Atmos. Chem. Phys., 15(16), 9577–9591, doi:10.5194/acp-15-9577-2015, 2015.

Bessagnet, B., Hodzic, A., Blanchard, O., Lattuati, M., Le Bihan, O., Marfaing, H. and Rou??l, L.: Origin of particulate matter pollution episodes in wintertime over the Paris Basin, Atmos. Environ., 39(33), 6159–6174,
25   doi:10.1016/j.atmosenv.2005.06.053, 2005.

Bressi, M., Sciare, J., Ghersi, V., Bonnaire, N., Nicolas, J. B., Petit, J. E., Moukhtar, S., Rosso, A., Mihalopoulos, N. and Féron, A.: A one-year comprehensive chemical characterisation of fine aerosol (PM2.5) at urban, suburban and rural background sites in the region of Paris (France), Atmos. Chem. Phys., 13(15), 7825–7844, doi:10.5194/acp-13-7825-2013, 2013.

30   Bressi, M., Sciare, J., Ghersi, V., Mihalopoulos, N., Petit, J.-E., Nicolas, J. B., Moukhtar, S., Rosso, A., Féron, A., Bonnaire, N., Poulakis, E. and Theodosi, C.: Sources and geographical origins of fine aerosols in Paris (France), Atmos. Chem. Phys., 14(16), 8813–8839, doi:10.5194/acp-14-8813-2014, 2014.

Chazette, P.: The monsoon aerosol extinction properties at Goa during INDOEX as measured with lidar, J. Geophys. Res., 108(D6), 4187, doi:10.1029/2002JD002074, 2003.

Chazette, P. and Royer, P.: Springtime major pollution events by aerosol over Paris Area: From a case study to a multiannual analysis, J. Geophys. Res. Atmos., 122(15), 8101–8119, doi:10.1002/2017JD026713, 2017.

5   Chazette, P. and Totems, J.: Mini N2-Raman Lidar onboard ultra-light aircraft for aerosol measurements: Demonstration and extrapolation, Remote Sens., 9(12), doi:10.3390/rs9121226, 2017.

Chazette, P., Randriamiarisoa, H., Sanak, J., Couvert, P. and Flamant, C.: Optical properties of urban aerosol from airborne and ground-based in situ measurements performed during the Etude et Simulation de la Qualité de l'air en Ile de France (ESQUIF) program, J. Geophys. Res., 110(D2), D02206, doi:10.1029/2004JD004810, 2005.

10 Chazette, P., Sanak, J. and Dulac, F.: Monsoon Multidisciplinary Analysis, , 8335–8341, 2007.

Chazette, P., Bocquet, M., Royer, P., Winiarek, V., Raut, J.-C., Labazuy, P., Gouhier, M., Lardier, M. and Cariou, J.-P.: Eyjafjallajökull ash concentrations derived from both lidar and modeling, J. Geophys. Res. Atmos., 117(4), doi:10.1029/2011JD015755, 2012a.

Chazette, P., Dabas, a., Sanak, J., Lardier, M. and Royer, P.: French airborne lidar measurements for Eyjafjallajökull ash
15 plume survey, Atmos. Chem. Phys., 12(15), 7059–7072, doi:10.5194/acp-12-7059-2012, 2012b.

Chazette, P., Totems, J., Ancellet, G., Pelon, J. and Sicard, M.: Temporal consistency of lidar observations during aerosol transport events in the framework of the ChArMEx/ADRIMED campaign at Minorca in June 2013, Atmos. Chem. Phys., 16(5), 2863–2875, doi:10.5194/acp-16-2863-2016, 2016.

Chew, B. N., Campbell, J. R., Reid, J. S., Giles, D. M., Welton, E. J., Salinas, S. V. and Liew, S. C.: Tropical cirrus cloud
20 contamination in sun photometer data, Atmos. Environ., 45(37), 6724–6731, doi:10.1016/j.atmosenv.2011.08.017, 2011.

Chu, Y., Liu, Y., Li, X., Liu, Z., Lu, H., Lu, Y., Mao, Z., Chen, X., Li, N., Ren, M., Liu, F., Tian, L., Zhu, Z. and Xiang, H.: A review on predicting ground PM2.5 concentration using satellite aerosol optical depth, Atmosphere (Basel)., 7(10), 1–25, doi:10.3390/atmos7100129, 2016.

Crippa, M., Canonaco, F., Slowik, J. G., El Haddad, I., Decarlo, P. F., Mohr, C., Heringa, M. F., Chirico, R., Marchand, N.,
25 Temime-Roussel, B., Abidi, E., Poulain, L., Wiedensohler, A., Baltensperger, U. and Prévôt, A. S. H.: Primary and secondary organic aerosol origin by combined gas-particle phase source apportionment, Atmos. Chem. Phys., 13(16), 8411–8426, doi:10.5194/acp-13-8411-2013, 2013a.

Crippa, M., Decarlo, P. F., Slowik, J. G., Mohr, C., Heringa, M. F., Chirico, R., Poulain, L., Freutel, F., Sciare, J., Cozic, J., Di Marco, C. F., Elsasser, M., Nicolas, J. B., Marchand, N., Abidi, E., Wiedensohler, A., Drewnick, F., Schneider, J.,
30 Borrmann, S., Nemitz, E., Zimmermann, R., Jaffrezo, J. L., Prévôt, A. S. H. and Baltensperger, U.: Wintertime aerosol chemical composition and source apportionment of the organic fraction in the metropolitan area of Paris, Atmos. Chem. Phys., 13(2), 961–981, doi:10.5194/acp-13-961-2013, 2013b.

Cros, B., Durand, P., Cachier, H., Drobinski, P., Fréjafon, E., Kottmeier, C., Perros, P. E., Peuch, V. H., Ponche, J. L., Robin, D., Saïd, F., Toupance, G. and Wortham, H.: The ESCOMPTE program: An overview, Atmos. Res.,

doi:10.1016/j.atmosres.2003.05.001, 2004.

Cuesta, J., Flamant, P. H. and Flamant, C.: Synergetic technique combining elastic backscatter lidar data and sunphotometer AERONET inversion for retrieval by layer of aerosol optical and microphysical properties, Appl. Opt., doi:10.1364/ao.47.004598, 2008.

5 Dieudonné, E., Chazette, P., Marnas, F., Totems, J. and Shang, X.: Lidar profiling of aerosol optical properties from Paris to Lake Baikal (Siberia), Atmos. Chem. Phys., 15(9), 5007–5026, doi:doi:10.5194/acp-15-5007-2015, 2015.

Dieudonné, E., Chazette, P., Marnas, F., Totems, J. and Shang, X.: Raman Lidar Observations of Aerosol Optical Properties in 11 Cities from France to Siberia, Remote Sens., 9(10), 978, doi:10.3390/rs9100978, 2017.

Dubovik, O., Smirnov, A., Holben, B. N., King, M. D., Kaufman, Y. J., Eck, T. F. and Slutsker, I.: Accuracy assessments of
10 aerosol optical properties retrieved from Aerosol Robotic Network (AERONET) Sun and sky radiance measurements, J. Geophys. Res. Atmos., 105(D8), 9791–9806, doi:10.1029/2000JD900040, 2000.

ECMWF: ERA5 data documentation, Eur. Cent. Mediu. Weather Forecast., 2017.

European Commission: Clean Air for Europe - Improving air quality Why care about air pollution? Ecosystems , climate , health , economy., 2015.

15 Flamant, P., Cuesta, J., Denneulin, M. L., Dabas, A. and Huber, D.: ADM-Aeolus retrieval algorithms for aerosol and cloud products, Tellus, Ser. A Dyn. Meteorol. Oceanogr., 60 A(2), 273–288, doi:10.1111/j.1600-0870.2007.00287.x, 2008.

Gupta, P., Christopher, S. A., Wang, J., Gehrig, R., Lee, Y. and Kumar, N.: Satellite remote sensing of particulate matter and air quality assessment over global cities, Atmos. Environ., 40(30), 5880–5892, doi:10.1016/j.atmosenv.2006.03.016, 2006.

Hersey, S. P., Craven, J. S., Metcalf, A. R., Lin, J., Lathem, T., Suski, K. J., Cahill, J. F., Duong, H. T., Sorooshian, A., Jonsson,
20 H. H., Shiraiwa, M., Zuend, A., Nenes, A., Prather, K. A., Flagan, R. C. and Seinfeld, J. H.: Composition and hygroscopicity ofthe Los Angeles Aerosol: CalNex, J. Geophys. Res. Atmos., doi:10.1002/jgrd.50307, 2013.

Hodzic, A., Chepfer, H., Vautard, R., Chazette, P., Beekmann, M., Bessagnet, B., Chatenet, B., Cuesta, J., Drobinski, P., Goloub, P., Haeffelin, M. and Morille, Y.: Comparison of aerosol chemistry transport model simulations with lidar and Sun photometer observations at a site near Paris, J. Geophys. Res. D Atmos., 109(23), doi:10.1029/2004JD004735, 2004.

25 Hodzic, A., Vautard, R., Chazette, P., Menut, L. and Bessagnet, B.: Aerosol chemical and optical properties over the Paris area within ESQUIF project, Atmos. Chem. Phys., 6(11), 3257–3280, doi:10.5194/acp-6-3257-2006, 2006.

Hogg, J. C. and Van Eeden, S.: Pulmonary and systemic response to atmospheric pollution, Respirology, 14(3), 336–346, doi:10.1111/j.1440-1843.2009.01497.x, 2009.

Holben, B. N., Eck, T. F., Slutsker, I., Tanré, D., Buis, J. P., Setzer, A., Vermote, E., Reagan, J. A., Kaufman, Y. J., Nakajima,
30 T., Lavenu, F., Jankowiak, I. and Smirnov, A.: AERONET—A Federated Instrument Network and Data Archive for Aerosol Characterization, Remote Sens. Environ., 66(1), 1–16, doi:10.1016/S0034-4257(98)00031-5, 1998.

IIASA: Loss in life expectancy attributable to exposure to fine particulate matter - 2000 Loss in life expectancy attributable to exposure to fine particulate matter – Baseline 2020., 2000.

Ile de France Prefecture, R.: Population statistics of Ile de France region, 2017.

Illingworth, A. J., Barker, H. W., Beljaars, A., Ceccaldi, M., Chepfer, H., Clerbaux, N., Cole, J., Delanoë, J., Domenech, C., Donovan, D. P., Fukuda, S., Hirakata, M., Hogan, R. J., Huenerbein, A., Kollias, P., Kubota, T., Nakajima, T., Nakajima, T. Y., Nishizawa, T., Ohno, Y., Okamoto, H., Oki, R., Sato, K., Satoh, M., Shephard, M. W., Velázquez-Blázquez, A., Wandinger, U., Wehr, T. and Van Zadelhoff, G. J.: The earthcare satellite : The next step forward in global measurements of clouds, aerosols, precipitation, and radiation, Bull. Am. Meteorol. Soc., 96(8), 1311–1332, doi:10.1175/BAMS-D-12-00227.1, 2015.

IPCC: Working Group I Contribution to the IPCC Fifth Assessment Report, Climate Change 2013: The Physical Science Basis., 2013.

Jaffrezo, J. L., Aymoz, G., Delaval, C. and Cozic, J.: Seasonal variations of the water soluble organic carbon mass fraction of aerosol in two valleys of the French Alps, Atmos. Chem. Phys., doi:10.5194/acp-5-2809-2005, 2005.

Kacenelenbogen, M.: Kacenelenbogen - 2006 - and Physics Characterization of aerosol pollution events in France using ground-based and POLDER-2 satellite data.pdf, , 2(November 1996), 4843–4849, 2006.

Kim, M.-H. H., Omar, A. H., Tackett, J. L., Vaughan, M. A., Winker, D. M., Trepte, C. R., Hu, Y., Liu, Z., Poole, L. R., Pitts, M. C., Kar, J. and Magill, B. E.: The CALIPSO version 4 automated aerosol classification and lidar ratio selection algorithm, Atmos. Meas. Tech., 11(11), 6107–6135, doi:10.5194/amt-11-6107-2018, 2018.

King, M. D., Kaufman, Y. J., Menzel, W. P. and Tanré, D.: Remote Sensing of Cloud, Aerosol, and Water Vapor Properties from MODIS, IEEE Trans. Geosci. Remote Sens., 30(1), 1992.

Koelemeijer, R. B. A., Homan, C. D. and Matthijsen, J.: Comparison of spatial and temporal variations of aerosol optical thickness and particulate matter over Europe, Atmos. Environ., 40(27), 5304–5315, doi:10.1016/j.atmosenv.2006.04.044, 2006.

Levy, R. C., Remer, L. A., Kleidman, R. G., Mattoo, S., Ichoku, C., Kahn, R. and Eck, T. F.: Global evaluation of the Collection 5 MODIS dark-target aerosol products over land, Atmos. Chem. Phys., 10(21), 10399–10420, doi:10.5194/acp-10-10399-2010, 2010.

Levy, R. C., Mattoo, S., Munchak, L. A., Remer, L. A., Sayer, A. M., Patadia, F. and Hsu, N. C.: The Collection 6 MODIS aerosol products over land and ocean, Atmos. Meas. Tech., 6(11), 2989–3034, doi:10.5194/amt-6-2989-2013, 2013.

Mamouri, R. E., Amiridis, V., Papayannis, A., Giannakaki, E., Tsaknakis, G. and Balis, D. S.: Validation of CALIPSO space-borne-derived attenuated backscatter coefficient profiles using a ground-based lidar in Athens, Greece, Atmos. Meas. Tech., 2(2), 513–522, doi:10.5194/amt-2-513-2009, 2009.

McMeeking, G. R. R., Bart, M., Chazette, P., Haywood, J. M. M., Hopkins, J. R. R., McQuaid, J. B. B., Morgan, W. T. T., Raut, J.-C., Ryder, C. L. L., Savage, N., Turnbull, K. and Coe, H.: Airborne measurements of trace gases and aerosols over the London metropolitan region, Atmos. Chem. Phys., 12(11), 5163–5187, doi:10.5194/acp-12-5163-2012, 2012.

Menut, L., Flamant, C. and Pelon, J.: Evidence of Interaction Between Synoptic and Local, , (June), 269–286, 1999a.

Menut, L., Flamant, C., Pelon, J. and Flamant, P. H.: Urban boundary layer height determination from lidar measurements over the Paris area, Appl. Opt., 38(6), 945–954, doi:10.1364/AO.38.000945, 1999b.

Molina, L. T., Madronich, S., Gaffney, J. S., Apel, E., de Foy, B., Fast, J., Ferrare, R., Herndon, S., Jimenez, J. L., Lamb, B., Osornio-Vargas, A. R., Russell, P., Schauer, J. J., Stevens, P. S., Volkamer, R. and Zavala, M.: An overview of the MILAGRO 2006 Campaign: Mexico City emissions and their transport and transformation, Atmos. Chem. Phys., 10(18), 8697–8760, doi:10.5194/acp-10-8697-2010, 2010.

5   Molina, M. J. and Molina, L. T.: Megacities and Atmospheric Pollution Megacities and Atmospheric Pollution, J. Air Waste Manage. Assoc., 54(June), 644–680, doi:10.1080/10473289.2004.10470936, 2004.

Müller, D., Ansmann, A., Mattis, I., Tesche, M., Wandinger, U., Althausen, D., Pisani, G. and M??ller, D.: Aerosol-type-dependent lidar ratios observed with Raman lidar, J. Geophys. Res. Atmos., 112(16), D16202, doi:10.1029/2006JD008292, 2007.

10   NASA: CATS L2O Profile Products Quality Statements., 2017.

OECD: The Economic Consequences of Outdoor Air Pollution: Policy Highlights, , 20, doi:10.1787/9789264257474-en, 2016.

Omar, A. H., Winker, D. M., Kittaka, C., Vaughan, M. A., Liu, Z., Hu, Y., Trepte, C. R., Rogers, R. R., Ferrare, R. A., Lee, K. P., Kuehn, R. E. and Hostetler, C. A.: The CALIPSO automated aerosol classification and lidar ratio selection algorithm, J. Atmos. Ocean. Technol., 26(10), 1994–2014, doi:10.1175/2009JTECHA1231.1, 2009.

15   Pahlow, M., Muller, D., Tesche, M., Eichler, H., Feingold, G., Eberhard, W. L. and Cheng, Y. F.: Retrieval of aerosol properties from combined multiwavelength lidar and sunphotometer measurements, Appl. Opt., 2006.

Pereira, R. H. M., Nadalin, V., Monasterio, L. and Albuquerque, P. H. M.: Urban Centrality: A Simple Index, Geogr. Anal., 45(1), 77–89, doi:10.1111/gean.12002, 2013.

Petit, J. E., Amodeo, T., Meleux, F., Bessagnet, B., Menut, L., Grenier, D., Pellan, Y., Ockler, A., Rocq, B., Gros, V., Sciare,

20   J. and Favez, O.: Characterising an intense PM pollution episode in March 2015 in France from multi-site approach and near real time data: Climatology, variabilities, geographical origins and model evaluation, Atmos. Environ., 155(March 2015), 68–84, doi:10.1016/j.atmosenv.2017.02.012, 2017.

Pikridas, M., Sciare, J., Freutel, F., Crumeyrolle, S. and Borbon, A.: In situ formation and spatial variability of particle number concentration in a European megacity, , 10219–10237, doi:10.5194/acp-15-10219-2015, 2015.

25   Proestakis, E., Amiridis, V., Marinou, E., Binietoglou, I., Ansmann, A., Wandinger, U., Hofer, J., Yorks, J., Nowottnick, E., Makhmudov, A., Papayannis, A., Pietruczuk, A., Gialitaki, A., Apituley, A., Szkop, A., Muñoz Porcar, C., Bortoli, D., Dionisi, D., Althausen, D., Mamali, D., Balis, D., Nicolae, D., Tetoni, E., Liberti, G. L., Baars, H., Mattis, I., Stachlewska, I., Voudouri, K. A., Mona, L., Mylonaki, M., Perrone, M. R., Costa, M. J., Sicard, M., Papagiannopoulos, N., Siomos, N., Burlizzi, P., Pauly, R., Engelmann, R., Abdullaev, S. and Pappalardo, G.: EARLINET evaluation of the CATS L2 aerosol backscatter

30   coefficient product, Atmos. Chem. Phys. Discuss., (February), 1–30, doi:10.5194/acp-2019-45, 2019.

Randriamiarisoa, H., Chazette, P., Couvert, P., Sanak, J. and Mégie, G.: Relative humidity impact on aerosol parameters in a Paris suburban area, Atmos. Chem. Phys., 6(5), 1389–1407, doi:10.5194/acp-6-1389-2006, 2006.

Raut, J.-C. and Chazette, P.: Retrieval of aerosol complex refractive index from a synergy between lidar, sunphotometer and in situ measurements during LISAIR experiment, Atmos. Chem. Phys., 7(2001), 2797–2815, 2007.

Raut, J. C. and Chazette, P.: Assessment of vertically-resolved PM10 from mobile lidar observations, Atmos. Chem. Phys., 9, 8617–8638, doi:10.5194/acp-9-8617-2009, 2009.

Remer, L. A., Kaufman, Y. J., Tanré, D., Mattoo, S., Chu, D. A., Martins, J. V., Li, R.-R., Ichoku, C., Levy, R. C., Kleidman, R. G., Eck, T. F., Vermote, E. and Holben, B. N.: The MODIS Aerosol Algorithm, Products, and Validation, J. Atmos. Sci., 62(4), 947–973, doi:10.1175/JAS3385.1, 2005.

Royer, P., Chazette, P., Lardier, M. and Sauvage, L.: Aerosol content survey by mini N2-Raman lidar: Application to local and long-range transport aerosols, Atmos. Environ., 45(39), 7487–7495, doi:10.1016/j.atmosenv.2010.11.001, 2011a.

Royer, P., Chazette, P., Sartelet, K., Zhang, Q. J., Beekmann, M. and Raut, J. C.: Comparison of lidar-derived PM10 with regional modeling and ground-based observations in the frame of MEGAPOLI experiment, Atmos. Chem. Phys., 11(20), 10705–10726, doi:10.5194/acp-11-10705-2011, 2011b.

Russo, F., Whiteman, D. N., Demoz, B. and Hoff, R. M.: Validation of the Raman lidar algorithm for quantifying aerosol extinction, Appl. Opt., doi:10.1364/ao.45.007073, 2006.

Salmonson, V. V., Barnes, W. L. L., Maymon, P. W. P. W. P. W., Montgomery, H. E. H. E. and Ostrow, H.: MODIS: Advanced Facility Instrument for Studies of the Earth as a System, IEEE Trans. Geosci. Remote Sens., 27(2), 145–153, doi:10.1109/36.20292, 1989.

Sciare, J., D'Argouges, O., Zhang, Q. J., Sarda-Estève, R., Gaimoz, C., Gros, V., Beekmann, M. and Sanchez, O.: Comparison between simulated and observed chemical composition of fine aerosols in Paris (France) during springtime: Contribution of regional versus continental emissions, Atmos. Chem. Phys., 10(24), 11987–12004, doi:10.5194/acp-10-11987-2010, 2010.

Skyllakou, K., Murphy, B. N., Megaritis, A. G., Fountoukis, C. and Pandis, S. N.: Contributions of local and regional sources to fine PM in the megacity of Paris, Atmos. Chem. Phys., 14(5), 2343–2352, doi:10.5194/acp-14-2343-2014, 2014.

Steeneveld, G.: Stable boundary layer issues, Met.Wau.Nl, (November), 7–10, 2011.

Stephens, G. L., Vane, D. G., Boain, R. J., Mace, G. G., Sassen, K., Wang, Z., Illingworth, A. J., O'Connor, E. J., Rossow, W. B., Durden, S. L., Miller, S. D., Austin, R. T., Benedetti, A., Mitrescu, C., CloudSat Science Team, T., Collins, F., City, S. L. and Kingdom, U.: The Cloudsat Mission and the A-Train, Bull. Am. Meteorol. Soc., (December 2002), 1771–1790, doi:10.1175/BAMS-83-12-1771, 2002.

Tombette, M., Mallet, V. and Sportisse, B.: PM₁₀ data assimilation over Europe with the optimal interpolation method, Atmos. Chem. Phys., 9(1), 57–70, doi:10.5194/acp-9-57-2009, 2009.

Toth, T. D., Zhang, J., Campbell, J. R., Hyer, E. J., Reid, J. S., Shi, Y. and Westphal, D. L.: Impact of data quality and surface-to-column representativeness on the PM 2.5 / satellite AOD relationship for the contiguous United States, Atmos. Chem. Phys, 14, 6049–6062, doi:10.5194/acp-14-6049-2014, 2014.

Vautard, R., Menut, L., Beekmann, M., Chazette, P., Flamant, P. H., Gombert, D., Guédalia, D., Kley, D., Lefebvre, M.-P., Martin, D., Mégie, G., Perros, P. and Toupance, G.: A synthesis of the Air Pollution Over the Paris Region (ESQUIF) field campaign, J. Geophys. Res., 108(D17), 8558, doi:10.1029/2003JD003380, 2003.

Wang, J. and Christopher, S. A.: Intercomparison between satellite-derived aerosol optical thickness and PM2.5mass:

Implications for air quality studies, Geophys. Res. Lett., 30(21), 2–5, doi:10.1029/2003GL018174, 2003.

Wang, Y., Sartelet, K. N. N., Bocquet, M. and Chazette, P.: Assimilation of ground versus lidar observations for PM10 forecasting, Atmos. Chem. Phys., 13(1), 269–283, doi:10.5194/acp-13-269-2013, 2013.

Wang, Y., Sartelet, K. N. N., Bocquet, M., Chazette, P., Sicard, M., D'Amico, G., Léon, J. F. F., Alados-Arboledas, L., Amodeo, A., Augustin, P., Bach, J., Belegante, L., Binietoglou, I., Bush, X., Comerón, A., Delbarre, H., García-Vízcaino, D., Guerrero-Rascado, J. L. L., Hervo, M., Iarlori, M., Kokkalis, P., Lange, D., Molero, F., Montoux, N., Muñoz, A., Muñoz, C., Nicolae, D., Papayannis, A., Pappalardo, G., Preissler, J., Rizi, V., Rocadenbosch, F., Sellegri, K., Wagner, F., Dulac, F., Rizi, V., Rocadenbosch, F., Sellegri, K., Wagner, F. and Dulac, F.: Assimilation of lidar signals: application to aerosol forecasting in the western Mediterranean basin, Atmos. Chem. Phys., 14(22), 12031–12053, doi:10.5194/acp-14-12031-2014, 2014.

Von Der Weiden-Reinmüller, S. L., Drewnick, F., Zhang, Q. J., Freutel, F., Beekmann, M. and Borrmann, S.: Megacity emission plume characteristics in summer and winter investigated by mobile aerosol and trace gas measurements: The Paris metropolitan area, Atmos. Chem. Phys., 14(23), 12931–12950, doi:10.5194/acp-14-12931-2014, 2014.

Winker, D. M., Pelon, J., Mccormick, M. P., Pierre, U. and Jussieu, P.: The CALIPSO mission : Spaceborne lidar for observation of aerosols and clouds, Proc. SPIE vol. 4893, 4893, 1–11, doi:10.1117/12.466539, 2003.

Yorks, J., Palm, S., McGill, M., Hlavka, D., Hart, W., Selmer, P. and Nowottnick, E.: CATS Algorithm Theoretical Basis Document Level 1 and Level 2 Data Products, , Release 1., 2015.